Experimental Neurology 317 (2019) 34–50

Contents lists available at ScienceDirect

Experimental Neurology

journal homepage: www.elsevier.com/locate/yexnr

Research paper

FGF21 promotes functional recovery after hypoxic-ischemic brain injury in neonatal rats by activating the PI3K/Akt signaling pathway via FGFR1/β-klotho

Lixia Ye[a], Xue Wang[b], Chenchen Cai[a], Shanshan Zeng[a], Junjie Bai[a], Kaiming Guo[b], Mingchu Fang[a], Jian Hu[b], Huan Liu[b], Liyun Zhu[b], Fei Liu[b], Dongxue Wang[b], Yingying Hu[a], Shulin Pan[a], Xiaokun Li[b], Li Lin[b,*], Zhenlang Lin[a,*]

[a] Department of Neonatology, The Second Affiliated Hospital and Yuying Children's Hospital, Wenzhou Medical University, Wenzhou, Zhejiang 325027, China
[b] School of Pharmaceutical Sciences, Wenzhou Medical University, Wenzhou, Zhejiang 325035, China

ARTICLE INFO

Keywords:
Neonatal hypoxic-ischemic brain injury
Functional recovery
Oxygen-glucose deprivation
FGF21
FGF21/FGFR1/β-klotho complex
PI3K/Akt

ABSTRACT

Perinatal asphyxia often results in neonatal cerebral hypoxia-ischemia (HI), which is associated with high mortality and severe long-term neurological deficits in newborns. Currently, there are no effective drugs to mitigate the functional impairments post-HI. Previous studies have shown that fibroblast growth factor 21 (FGF21) has a potential neuroprotective effect against brain injury. However, the effect of FGF21 on neonatal HI brain injury is unclear. In the present study, both in vivo and in vitro models were used to assess whether recombinant human FGF21 (rhFGF21) could exert a neuroprotective effect after HI and explore the associated mechanism. The results showed that the rhFGF21 treatment remarkably reduced the infarct volume, ameliorated the body weight and improved the tissue structure after HI in neonatal rats. In addition, the rhFGF21 treatment lengthened the running endurance times in the rotarod test and decreased the mean escape latencies and increased the number of platform crossings in the Morris water maze test at 21 d post-HI insult. In contrast, the FGFR1 inhibitor PD173074 and PI3K inhibitor LY294002 partially reversed these therapeutic effects. In isolated primary cortical neurons, the rhFGF21 treatment protected primary neurons from oxygen-glucose deprivation (OGD) insult by inhibiting neuronal apoptosis and promoting neuronal survival. Both our in vivo and in vitro results reveal that rhFGF21 could inhibit neuronal apoptosis by activating the PI3K/Akt signaling pathway via FGF21/FGFR1/β-klotho complex formation. Therefore, rhFGF21 may be a promising therapeutic agent for promoting functional recovery after HI-induced neonatal brain injury.

1. Introduction

Although antenatal and neonatal care has advanced in recent years, hypoxia-ischemia (HI) induced neonatal brain injury is a major cause of high mortality among newborns. The reported incidence is 1–8/1000 live births in developed countries and up to approximately 26/1000 live births in underdeveloped countries (Yıldız et al., 2016). Babies surviving hypoxic-ischemic encephalopathy (HIE) have life-long neurological deficits, including cerebral palsy, visual and auditory problems, and motor and behavioral damages (Al-Macki et al., 2009; Ma and Zhang, 2018). Currently, there are no effective clinical therapies except for therapeutic hypothermia, which has been regarded as the only reliable standard therapy for infants with HIE (Zalewska et al., 2015). Hypothermia notably reduces morbidity and mortality from HIE, but some patients still die, or survive with sequelae according to long-term follow-up (Silveira and Procianoy, 2015). Thus, exploring more effective treatment strategies is necessary to ameliorate neurological deficits after HI injury.

The pathogenesis of neonatal HI brain injury is complex and involves excitotoxicity, mitochondrial damage, oxidative stress,

Abbreviations: HI, hypoxia-ischemia; HIE, hypoxic-ischemic encephalopathy; FGF21, fibroblast growth factor 21; rhFGF21, recombinant human FGF21; CNS, central nervous system; OGD, oxygen-glucose deprivation; BBB, blood-brain barrier; FGFR, FGF receptors; DMSO, dimethylsulfoxide; ip, intraperitoneal; icv, intracerebroventricular; TTC, 2,3,5-triphenyltetrazolium chloride; CBF, cerebral blood flow; rCBF, regional cerebral blood flow; ROI, region of interest; MWM, Morris water maze; MAP-2, microtubule-associated protein-2

* Corresponding authors.
E-mail addresses: linliwz@163.com (L. Lin), linzhenlang@hotmail.com (Z. Lin).

https://doi.org/10.1016/j.expneurol.2019.02.013
Received 21 December 2018; Received in revised form 10 February 2019; Accepted 21 February 2019
Available online 23 February 2019
0014-4886/

inflammation, and apoptosis (Douglas-Escobar and Weiss, 2015). Apoptosis begins during the early phase of the injury and can last for days or weeks after the HI brain insult (Northington et al., 2005). Neuronal apoptosis plays an important role in HI-induced neuronal loss, especially in the penumbra area (Tu et al., 2018). Therefore, reducing apoptosis and increasing neuronal survival can serve as effective therapeutic targets for neonatal HI brain injury.

Fibroblast growth factor 21 (FGF21) is an endocrine FGF that consists of 209 amino acids and is widely expressed in metabolic organs, including the pancreas, liver, gut and adipose tissue (Fon Tacer et al., 2010). FGF21 is also expressed in brain regions, including the substantia nigra, striatum, hippocampus and cortex (Mäkelä et al., 2014). Plasma FGF21 can reportedly cross the blood-brain barrier (BBB) by simple diffusion (Hsuchou et al., 2007). In contrast to the classical FGFs, FGF21 does not require heparin for receptor binding (Kharitonenkov, 2009), and does not exhibit mitogen activity (Xie and Leung, 2017). In contrast, FGF21 binding to FGF receptors (FGFRs) requires a co-receptor called β-klotho, which is a single-pass transmembrane protein (Adams et al., 2012; Kharitonenkov, 2009). FGF21 binds FGFR with its N-terminus and β-klotho with its C-terminus to form a stable FGF21/FGFR/β-klotho complex(Kharitonenkov, 2009), which activates downstream signaling pathways, including the RAS-RAF-mitogen-activation protein kinase (MAPK), signal transducers and activators of transcription (STATs), and phosphatidylinositol 3-kinase (PI3K)-serine-threonine protein kinase (Akt) pathways (Itoh and Ornitz, 2011). The PI3K/Akt signaling pathway participates in many vital cellular processes, including cell survival/apoptosis, proliferation and differentiation (Xiong et al., 2012). Akt phosphorylation (p-Akt), especially in the ischemic penumbra, is observed early after cerebral ischemia in both adults and neonates (Zhang et al., 2015). Pan et al. (2018) reported that FGF21 prevents type 2 diabetes by promoting insulin synthesis and secretion, which is partially attributed to the activation of PI3K/Akt signaling. Other studies have demonstrated that PI3K/Akt pathway activation is involved in the protective effect of FGF21 against myocardial ischemia-reperfusion injury (Cong et al., 2013; Hu et al., 2017). Thus, here, we mainly investigate the possible beneficial effects of PI3K/Akt signaling pathway activation by FGF21 on HI brain injury.

Various studies have suggested that FGF21 performs a pleiotropic function in glucose and lipid metabolism, insulin sensitivity and body weight (Kharitonenkov, 2009; Kharitonenkov et al., 2007). FGF21 has also been proven to regulate inflammatory responses (Wang et al., 2018a) and prevent oxidative stress (Cong et al., 2013; Planavila et al., 2015). Furthermore, growing evidence has revealed the potential role of FGF21 in central nervous system (CNS) diseases. A recent study demonstrated that peripherally derived FGF21 promotes remyelination in mice following toxin-induced demyelination (Kuroda et al., 2017). Mäkelä et al. (2014) reported that FGF21 increases mitochondrial efficacy in human dopaminergic neurons. Our previous study demonstrated that FGF21 protects against cerebral ischemia and decreases endoplasmic reticulum stress-related protein expression in adult rats following ischemic brain injury (Yang et al., 2018). We further found that FGF21 preserved the BBB integrity after traumatic brain injury (TBI) in mice (Chen et al., 2018b). Thus far, FGF21 therapy does not appear to result in harmful side effects, such as hypoglycemia, edema or liver toxicity (Xie and Leung, 2017), and FGF21 does not affect cell proliferation and tumourigenesis (Kharitonenkov et al., 2007). This evidence further confirms the safety of using FGF21 for the treatment of brain injury. Although studies have increasingly begun to focus on the relationship between FGF21 and brain function, the specific mechanism and targets of FGF21 in neonatal HI brain injury are still unclear.

In the present study, we performed both in vivo and in vitro experiments to explore whether exogenous FGF21 could play a neuroprotective role after HI injury and determine its relationship with the PI3K/Akt signaling pathway. Recombinant human FGF21 (rhFGF21) was administered to rats post-HI injury or primary cortical neurons after oxygen-glucose deprivation (OGD) insult. Furthermore, we used corresponding inhibitors to explore the potential mechanisms by which the rhFGF21 treatment attenuates neuronal death and neurofunctional deficits.

2. Materials and methods

2.1. Neonatal HI brain injury model and drugs administration

All animal care and experiments were conducted in strict accordance with the Guidelines for the Care and Use of Laboratory Animals by the National Institutes of Health and approved by the Laboratory Animal Ethics Committee of Wenzhou Medical University. All Sprague Dawley (SD) rats (200–250 g) were purchased from the Animal Center of the Chinese Academy of Science (Shanghai, China) and housed under specific pathogen-free conditions at the laboratory animal center. Adult rats mated freely to produce offspring for the subsequent studies. A modified Rice-Vannucci model was generated as previously described (Taniguchi and Andreasson, 2008). Postnatal day 7 (P 7) male rat pups were fully anesthetized with isoflurane (3%–4% for induction and 1%–2% for maintenance). The left common carotid artery was ligated and cut off to prevent vascular recanalization. After the surgery, the pups were returned to their dam and allowed to recuperate for 1–2 h. Then, the pups were placed in a hypoxia chamber (XBS-03, AIPU, HangZhou, China) for 2.5 h; the oxygen concentration was automatically maintained at 8% through pure nitrogen input at a flow rate of 1 L/min. The pups were placed on an electric blanket at a constant temperature of 37 °C during the hypoxic period. The pups were returned to their dam after 2.5 h of hypoxia. In the sham group, the left common carotid artery was exposed without actual artery ligature or hypoxia. The survival rate of the animals was 94%.

Recombinant human FGF21 (rhFGF21) was provided by the Key Laboratory of Biotechnology Pharmaceutical Engineering at Wenzhou Medical University, China. RhFGF21 was dissolved in a sterile 0.9% normal saline solution. The rats were randomly assigned to different experimental groups. To determine the best effective dose, the rhFGF21-treated HI group received different doses of rhFGF21 (0.75 mg/kg, 1.5 mg/kg, and 3 mg/kg) immediately after hypoxia by intraperitoneal (ip) injection at 24-h intervals for 3 d. Simultaneously, the rats in the vehicle-treated HI group received an equal volume of sterile 0.9% normal saline. To further assess whether rhFGF21 activated FGFR1/β-klotho and upregulated the PI3K/Akt pathway, the FGFR1 inhibitor PD173074 and PI3K inhibitor LY294002 (Selleck, Shanghai, China) were dissolved in 1% dimethylsulfoxide (DMSO) and used. Both inhibitors were administered via intracerebroventricular (icv) injection 30 min before HI using a stereotaxic apparatus (68045, RWD, China). For this purpose, 5 μL PD173074 (0.5 nmol/kg) or LY294002 (50 nmol/kg) (Huang et al., 2012) were injected into the lateral ventricle (2 mm rostral, 1.5 mm lateral to bregma, and 2.5 mm below the skull surface) (Harding et al., 2016; Zhou et al., 2017) at a rate of 1 μL/min. After the complete injection, the needle remained in place for an additional 10 min and then withdrawn at a rate of 1 mm/min. To prevent DMSO from interfering with the final results, 1% DMSO dissolved in a sterile saline solution (5 μL, icv) was injected 30 min before HI in the DMSO-treated sham, DMSO-treated HI and HI + rhFGF21 + DMSO groups. To evaluate the long-term outcomes, doses of 1.5 mg/kg rhFGF21 (ip) with PD173074 (0.5 nmol/kg) or LY294002 (50 nmol/kg) (icv) were administered at 24-h intervals for 7 d.

2.2. Infarct volume measurement

The infarct volume was measured by 2,3,5-triphenyltetrazolium chloride (TTC) staining as previously described (Li et al., 2012; Taniguchi and Andreasson, 2008). Then, 3 d after the HI injury, the pups were deeply anesthetized, and the brain tissue was perfused with cold normal saline and sectioned into 2-mm-thick coronal slices. A

solution of cold 1% TTC (Sigma Aldrich, St. Louis, MO USA) dissolved in phosphate-buffered saline was prepared and protected from light exposure. The brain slices were immersed in the 1% TTC solution in the dark for 30 min at 37 °C, followed by fixation in 4% paraformaldehyde (PFA) overnight. The brain infarct volume was traced and analyzed using ImageJ software (National Institutes of Health, Bethesda, MD, USA) and calculated by the formula described by Chen et al. (2018a).

2.3. Laser speckle contrast imaging

The cerebral blood flow (CBF) was measured through the intact parietal bone with the aid of laser speckle contrast imaging (PeriCam PSI, Perimed, Järfälla, Sweden). This technique provides a perfusion index proportional to the concentration and mean velocity of red blood cells, allowing for the monitoring of microvascular blood flow in real time (Humeau-Heurtier et al., 2015). The laser speckle contrast imaging tests were performed according to a previous study (Yuan et al., 2018). Briefly, 24 h post-HI injury, the pups' scalps were cut to expose the skulls sufficiently after isoflurane inhalation anesthesia (3%–4% for induction and 1%–2% for maintenance). Then, the pups were placed under a laser beam at a 785-nm wavelength, and raw speckle images were captured by a camera positioned 10 cm above the rats' heads. During the measurement, the pups were placed on an electric blanket at a constant temperature of 37 °C. The analysis of the laser speckle images and the relative CBF in the region of interest (ROI) was performed using Perisoft software (Perimed, Järfälla, Sweden). After completing the measurements, the scalps were sewn, and the pups were returned to their dams after recovery from anesthesia.

2.4. Western blot analysis

The rats were euthanized by deep anesthesia with isoflurane 4 h, 24 h, or 7 d after HI injury, and the cortex and hippocampus were separated and stored at −80 °C until analysis. Primary cortical neurons were scraped from the plates 1 h or 24 h after OGD. The total protein was extracted from the brain tissues and neurons using protein extraction reagents containing 1% protease and phosphatase inhibitors (P1260, Solarbio). Then, the protein concentrations were measured by a BCA protein assay kit (Solarbio). Equivalent amounts of protein (80 μg in vivo and 60 μg in vitro) were loaded and separated on 10% SDS-PAGE gels and then transferred to PVDF membranes (Bio-Rad, Hercules, CA, USA). After blocking with 5% nonfat milk for 2 h at room temperature, the membranes were incubated with primary antibodies overnight at 4 °C. The primary antibodies used included p-FGFR1 (1:1000, ab59194, Abcam), FGFR1 (1:400, ab10646, Abcam), β-klotho (1:1000, ab106794, Abcam), p-Akt (1:1000, #9271 L, Cell Signaling Technology), Akt (1:1000, #9272S, Cell Signaling Technology), Bcl-2 (1:1000, #2876, Cell Signaling Technology), cleaved caspase 3 (1:1000, #9664S, Cell Signaling Technology), MAP-2 (1:1000, ab11267, Abcam), and β-Actin (13000, AP0060, Bioworld). After washing with Tris-buffered saline and Tween 20 (TBST) three times, the membranes were incubated with the appropriate secondary antibodies (goat anti-mouse, 1:10,000, BS12478, Bioworld; goat anti-rabbit, 1:30,000, ab6721) for 1 h at room temperature. The bands were detected using a ChemiDoc XRS + Imaging System (Bio-Rad). The gray values of the bands were analyzed using Image Lab 5.0 software (Bio-Rad). All experiments were repeated at least three times.

2.5. TUNEL staining

Apoptotic DNA fragmentation was detected using the In Situ Cell Death Detection Kit (Roche, South San Francisco, CA, USA). In vivo, TUNEL staining was performed 3 d after the HI injury. The brain sections (5 μm thickness) were deparaffinized, rehydrated and incubated with 20 μg/mL proteinase K working solution (ST533, Beyotime) for 15–30 min at 37 °C. In vitro, 24 h after the OGD injury, the primary cortical neurons cultured in 24-well plates were fixed with 4% PFA for 1 h and then incubated with 0.1% Triton X-100 in 0.1% sodium citrate for 2 min on ice. Both in vivo and in vitro, apoptotic cells were stained with a TUNEL reaction mixture in a dark humidified chamber for 1 h at 37 °C. The negative controls were treated with only the labeling solution. After washing three times with PBS, DAPI was added for 7 min at room temperature. All apoptotic changes were evaluated under a Nikon ECLIPSETi microscope (Nikon, Tokyo, Japan). The apoptotic cells were characterized by green fluorescence, and the DAPI-labeled blue nuclei indicated the total number of cells. ImageJ software was used to quantitatively calculate the ratio of the number of TUNEL-positive cells to the total number of cells.

2.6. Histological staining

Seven days after the HI injury, the rats were euthanized by deep anesthesia with isoflurane and subjected to cardiac perfusion with 20 mL of normal saline, followed by perfusion with 20 mL of 4% PFA. The rat brains were postfixed in 4% PFA overnight at 4 °C. After gradient dehydration using ethanol and xylene, the brains were embedded in paraffin and sectioned into 5 μm-thick coronal slices for subsequent staining. Hematoxylin-eosin (HE) and Nissl staining were performed to observe the histopathological changes based on the manufacturer's protocol. The images were acquired using light microscopy. To quantify the extent of brain atrophy, the HE-stained coronal brain sections were analyzed by ImageJ software. The residual volume was calculated by the following formula: (ipsilateral hemisphere volume /contralateral hemisphere volume) × 100%. To quantify the neuronal density in the ipsilateral cortex and hippocampus (CA3 sector and DG), the HE and Nissl-stained brain sections were analyzed by Image-pro Plus 6.0 software (Media Cybernetics, United States).

2.7. Immunohistochemical staining

For the immunohistochemical staining, the brain sections were dried at 62 °C for 1 h, followed by xylene deparaffination, ethanol rehydration and incubation with 3% H_2O_2 (30% H_2O_2 diluted in 80% methanol) for 10 min. Then, the sections were boiled in citrate buffer for 2 min for the antigen retrieval. After cooling, the sections were blocked with 5% bovine serum albumin (BSA) dissolved in PBS for 30 min at 37 °C and incubated with a MAP-2 antibody (1:400, ab11267, Abcam) dissolved in 1% BSA overnight at 4 °C. Subsequently, the sections were treated with a goat anti-mouse secondary antibody (1:1000, BS12478, Bioworld) for 2 h at 37 °C, counter stained with hematoxylin for 2 min, and colored with a DAB kit (ZLI-9018, ZSGB-BIO). The images were captured using white light under a Nikon ECLIPSE 80i microscope (Nikon, Tokyo, Japan) and analyzed using ImageJ software. The percent of ipsilateral MAP-2-positive area loss was calculated using the following formula: [1- (area of ipsilateral MAP-2 staining/area of contralateral MAP-2 staining)] × 100%. In addition, ImageJ software was used to analyze the intensity of the MAP-2 positive staining in the tissue sections. Furthermore, the average integrated optical density (IOD) per stained area (IOD/area) of positive staining was calculated.

2.8. Neurobehavioral tests

The following neurobehavioral tests were performed in a double-blinded manner 3 weeks post-HI injury.

2.8.1. Rotarod performance test

To evaluate motor coordination, the rotarod test was performed using a rotarod apparatus (Ugo Basile 47750, Comerio, Italy) 3 weeks post-HI injury as previously described (Nakanishi et al., 2017). The rats were placed on the rod and forced to move to prevent falling. Before the start of the experiment, each rat was trained to adapt to the rotation at a fixed speed of 10 rpm for 10 s. After the training, the rotation of the rod

was gradually accelerated from 10 rpm to 40 rpm for 300 s, and the running time was recorded by the apparatus. The time recording did not stop until the animals fell from the rotating rod. The duration of this running time is called the endurance time. If an animal continued to run for longer than 180 s, the test was terminated, and the endurance time was considered 180 s. The tests were performed 3 times with a 30 min break between each test.

2.8.2. Morris water maze test

The Morris water maze (MWM) test is an experiment that forces animals to swim to find a platform hidden underwater. This test is mainly used to test the ability of experimental animals to learn and memorize spatial location and orientation. The MWM test was conducted 3 weeks after the HI insult as previously described (Grandvuillemin et al., 2017). Briefly, the rats swam in a black circular pool that was 140 cm in diameter and 50 cm in height filled with water to a height of 2 cm above the top of the movable platform, which had a diameter of 15 cm. The water was dyed black with nontoxic black ink. The pool was divided into four equal quadrants and located in a room protected from light and noise. The MWM testing began at 9 a.m. each morning and lasted for 6 d. The paths and data were recorded by a DigBhv animal behavioral analysis system.

2.8.2.1. Spatial acquisition test. The platform was placed in the southwest quadrant of the pool and submerged approximately 2 cm below the water surface. Spatial acquisition testing was conducted over five consecutive days. On each day, each rat performed three training trial swims starting from the three quadrants that were not the southwest quadrant where the platform was located. During each training session, the rats swam until they found the platform, and their escape latencies were recorded by the software. The rats that did not find the platform within 60 s were guided to the platform by the experimenter and allowed 30 s to orient before the next training. The average time required for the rats to find the platform was calculated as the learning score of each day. After testing, each rat was dried with a towel and placed under an infrared heat lamp before returning to its homecage.

2.8.2.2. Reference memory test (probe trial). To assess the spatial memory of the rats, the platform was removed 24 h after the final training. Each rat was placed in the northeast quadrant and allowed to swim freely for 60 s. The frequency of crossing the original platform location was recorded. After the trial, each rat was dried with a towel and placed under an infrared heat lamp before returning to its home cage.

2.9. Primary cortical neuron cultures

The primary cortical neurons were prepared from embryonal brains (E16–18 d) of SD rats as previously described (Chen et al., 2016, 2017a). Briefly, the cerebral cortices from embryonic rats were mechanically separated and placed in Hanks' balanced salt solution. After digestion in 0.25% trypsin-EDTA (Gibco, 25200-027) for 15 min at 37 °C, the triturated cortical tissue was filtered by a 70-μm cells trainer. The cell suspensions were seeded at 3×10^5 cells/mL in 6-well, 24-well and 96-well cell culture plates coated with poly-D-lysine (Sigma, P6407) overnight. The plates were cultured at 37 °C with 5% CO_2. The harvested cells were cultured in DMEM containing 10% FBS and 1% penicillin/streptomycin for < 24 h before the medium was changed to neurobasal medium (Gibco, 21103-049) containing 2% B27 (Gibco, 17504-044), 0.5 mM L-glutamine (Sigma, 49419) and 1% penicillin/streptomycin.

2.10. OGD and reoxygenation

The primary cortical neurons were subjected to OGD insult for 2 h on day 8 of the in vitro culture. Briefly, the culture medium was replaced with glucose-free DMEM, and the plates were placed in an enclosed anaerobic container. A mixed gas consisting of 95% N_2 and 5% CO_2 was continuously pumped into the anaerobic container for 2 h at 37 °C. After the OGD, the culture medium was replaced with neurobasal medium, and rhFGF21 (10 nM) with or without PD173074 (10 nM) or LY294002 (10 μM) was added. RhFGF21 was diluted in sterile purified water. PD173074 and LY294002 were dissolved in DMSO; the final concentration of DMSO in the medium was 0.02%. The plates were continually cultured in a normoxic incubator maintained at 37 °C and 5% CO_2 for reoxygenation for 24 h. In the control group, the neurons were cultured under normal conditions without oxygen or glucose deprivation.

2.11. Cell counting Kit-8 (CCK8) assay

To determine whether rhFGF21 could ameliorate OGD-induced cell death, Cell Counting Kit-8 (C0038, Beyotime, China) assays were used to evaluate the neuronal viability according to the manufacturer's instructions. The cells were plated in 96-well plates at a density of 3×10^4 cells/well. Different doses of rhFGF21 (0, 5, 10, and 50 nM) were added after OGD. After reoxygenation for 24 h, 10 μL of CCK-8 solution per well was added to the cells, which were then incubated in the dark for 4 h at 37 °C. The optical density (OD) was measured at 450 nm (Synergy H1, BioTek, USA), and the results are expressed as the percentages of live cells compared to those in the control group.

2.12. Immunofluorescence staining

One hour after the OGD injury, the primary cortical neuronscultured in 24-well plates were fixed with 4% PFA for 30 min and blocked with 5% BSA/0.3% Triton X-100 dissolved in PBS for 1 h at 37 °C. Then, the neurons were incubated with the following two primary antibodies over night: p-FGFR1 (1:200, ab59194, Abcam) and β-klotho (1:100, ab106794, Abcam). On the following day, the neurons were incubated with the following secondary antibodies for 1 h at 37 °C in the dark: AlexaFluor 488 goat anti-rabbit (1:1000, ab150077, Abcam) and TRITC goat anti-rabbit (1:1000, ab6718, Abcam). Then, the nuclei were labeled with DAPI for 7 min. All images were observed under a Nikon ECLIPSE Ti microscope (Nikon, Tokyo, Japan).

2.13. Statistical analysis

The quantitative data analysis is presented as the mean ± SEM of at least three independent experiments. Statistical significance was determined by one-way analysis of variance (ANOVA) followed by Tukey's test when analyzing more than two groups. Student's t-test was used for the comparisons of two groups. All statistical analyses were performed using GraphPad Prism 7.0 (GraphPad Software Inc., San Diego, CA, USA). $P < .05$ was considered significant.

3. Results

3.1. Intraperitoneal injection of rhFGF21 reduces the infarct volume post-HI injury

First, to verify the success of our HI model, we used laser speckle contrast imaging to dynamically monitor the cerebral blood flow (CBF) on the cortex surface 24 h after HI (Fig. 1a). Using this method, we obtained differences in regional CBF (rCBF) in the regions of interest (ROIs) in the bilateral hemispheres. The results showed that the difference in the bilateral rCBFin the sham group was −5.12 ± 1.12%, representing a negligible difference. However, the ipsilateral rCBF was decreased to −22.14 ± 1.19% compared with the contralateral rCBF post-HI injury (Fig. 1b). These data reveal that left common carotid artery ligation followed by systemic hypoxia could significantly decrease the rats' cerebral perfusion 24 h after the HI injury.

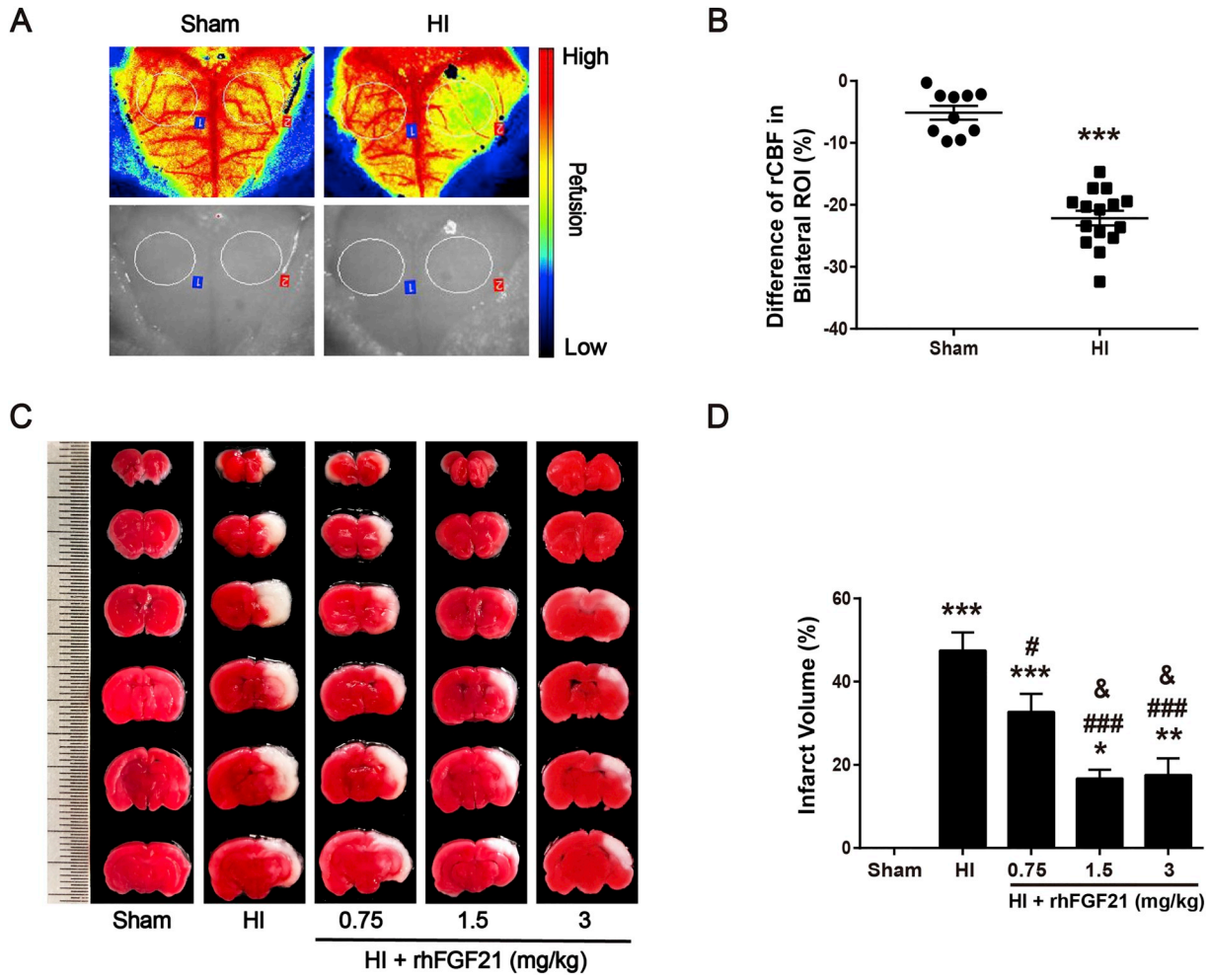

Fig. 1. Intraperitoneal injection of rhFGF21 reduced brain infarction 3 d post-HI. (a) Representative CBF images of the brain cortex and corresponding physical brain maps of rats were obtained by laser speckle contrast imaging 24 h after HI. The ROIs used for the CBF assessment are outlined in white in the images. (b) Quantification of CBF in bilateral ROIs. $^{***}P < .001$ vs. the sham group. The values represent the mean ± SEM. n = 10 in the sham group; n = 15 in the vehicle-treated HI group. (c) Representative photographs of TTC-stained coronal brain sections 3 d after HI. (d) Quantitative analysis of brain infarct volumes. $^{*}P < .05$, $^{**}P < .01$, and $^{***}P < .001$ vs. the sham group; $^{\#}P < .05$ and $^{\#\#\#}P < .001$ vs. the vehicle-treated HI group. $^{\&}P < .05$ vs. the HI + rhFGF21 (0.75 mg/kg) group. The values represent the mean ± SEM, n = 6.

To investigate whether rhFGF21 could alleviate the HI brain damage and determine the best effective dose, 0.75 mg/kg, 1.5 mg/kg and 3 mg/kg rhFGF21 were administered by intraperitoneal injection once per day for 3 d after HI. The cerebral infarct volume was evaluated by TTC staining 3 d after injury (Fig. 1c). The quantitative analysis of the TTC-stained sections revealed that compared to the vehicle treatment, 0.75 mg/kg rhFGF21 reduced the infarct volume (32.73 ± 4.33% vs. 47.48 ± 4.33%, $P < .05$). In contrast, we found that the brain-protecting effects of 1.5 mg/kg and 3 mg/kg rhFGF21 were superior to those of 0.75 mg/kg rhFGF21; these doses notably decreased the infarct volume to 16.72 ± 2.11% and 17.57 ± 4.02% (Fig. 1d). There was no significant difference in the infarct volume between these two concentrations. Therefore, rhFGF21 could effectively lessen the infarct extent after HI, and 1.5 mg/kg was the best concentration for the subsequent experiments.

3.2. rhFGF21 (1.5 mg/kg) treatment alleviates brain atrophy and increases body weight post-HI injury

Subsequently, we observed the anatomical structure of the brain 7 d post-HI injury (P 14). In the injured hemisphere, we found severe brain atrophy and even liquefaction. After the rhFGF21 treatment, the liquefaction extent was alleviated, but slight atrophy was still observed (Fig. 2a). The degree of brain atrophy in the different groups was quantitatively analyzed by HE staining of coronal brain sections 7 d post-HI (Fig. 2b). Compared with the sham group, the HI injury resulted in a significant brain volume loss of nearly 50% (98.1 ± 2.12% vs. 58.98 ± 4.12%, $P < .001$), whereas the rhFGF21 treatment increased the residual brain volume to 77.52 ± 5.09% (Fig. 2c). We monitored the body weights of the pups at different time points (P 7, P 14, P 21, and P 28) as an indicator of their general health level. There were no statistically significant differences in body weight among the three groups before the operation (P 7). The weight of the vehicle-treated HI group was lower than that of the sham group at each time point after the HI injury. However, the weight increased after the rhFGF21 treatment at all time points post-HI compared with the vehicle-treated rats (Fig. 2d), highlighting the drug safety of rhFGF21. These data suggest that the rhFGF21 treatment alleviated brain atrophy and improved the health of the rat pups after the HI injury.

3.3. rhFGF21 inhibits HI-induced neuronal apoptosis by activating the PI3K/Akt signaling pathway via FGFR1/β-klotho

FGF21 activates multiple FGFRs, and binds FGFR1 with a much higher affinity than the other FGFR subtypes in the presence of β-klotho (Xie and Leung, 2017). Thus, we performed western blotting to examine

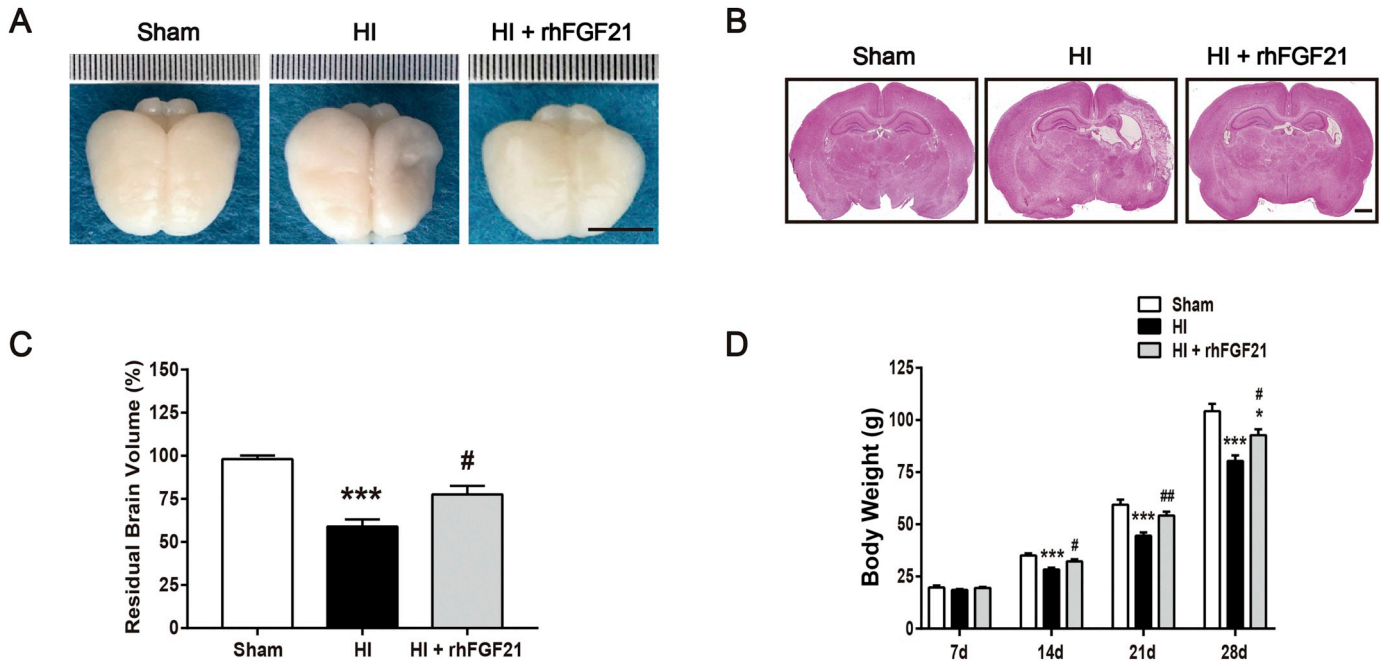

Fig. 2. rhFGF21 treatment mitigated brain atrophy and increased body weight post-HI injury. (a) Representative images of the anatomical structure of the rat brains 7 d post-HI injury. Scale bar = 1 cm. (b) Representative photographs of HE-stained coronal brain sections 7 d post HI. Scale bar = 1 mm. (c) The residual brain volume was defined as the ratio of the ipsilateral hemisphere to the contralateral hemisphere. $^{***}P < .001$ vs. the sham group; $^{\#}P < .05$ vs. the vehicle-treated HI group. The values represent the mean ± SEM, n = 6. (e) Body weight was measured at P 7, P 14, P 21, and P 28. $^{*}P < .05$ and $^{***}P < .001$ vs. the sham group; $^{\#}P < .05$ and $^{\#\#}P < .01$ vs. the vehicle-treated HI group. The values represent the mean ± SEM, n = 10.

whether rhFGF21 activates the FGFR1/β-klotho receptor complex. To further illustrate this effect, the FGFR1 inhibitor PD173074 was utilized 30 min before HI. As expected, rhFGF21 upregulated the expression of p-FGFR1 and β-klotho in the cortex and hippocampus 4 h post-HI. These effects were entirely reversed by PD173074 (Fig. 3a–c). To demonstrate that Akt was downstream of the FGFR1/β-klotho receptor complex, we measured the p-Akt and Akt levels by western blotting. The results showed that the protein expression of p-Akt was decreased 24 h after HI, while rhFGF21 significantly increased the p-Akt/Akt ratio. Nevertheless, PD173074 reversed the rhFGF21-induced upregulation of p-Akt, and the total Akt levels remained unchanged (Fig. 3d, e). Apoptosis is a primary cause of neuronal death and neurological deficits in neonatal HI brain damage (Zhu et al., 2005). Therefore, we investigated whether rhFGF21 could alleviate neuronal apoptosis after HI brain injury. At 3 d post-HI, we detected the expression of two apoptosis-related proteins (cleaved caspase 3 and Bcl-2) by performing a western blot analysis. To further demonstrate that Akt participated in the anti-apoptotic effect of rhFGF21, the PI3K inhibitor LY294002 was applied. The data revealed that the rhFGF21 treatment distinctly reversed the HI-induced increase in cleaved caspase 3 expression and the decrease in the expression of the anti-apoptotic protein Bcl-2, and this effect was partially inhibited by the LY294002 and PD173074 treatment (Fig. 3f–h).

TUNEL and TTC staining were performed 3 d post-HI. The TUNEL staining showed that in both the cortex and hippocampal CA3 region, the number of TUNEL-positive cells was clearly increased (Fig. 4a). However, the rhFGF21 treatment reduced the number of TUNEL-positive cells from 82.72 ± 1.63% to 37.25 ± 7.99% and from 44.52 ± 3.58% to 21.3 ± 3.49% in the cortex (Fig. 4b) and hippocampal CA3 region (Fig. 4c), respectively. Compared with the rhFGF21 treatment alone, the treatment with rhFGF21 plus PD173074 or LY294002 clearly increased the number of TUNEL-positive cells in the cortex and hippocampal CA3 region (Fig. 4a–c). Additionally, the TTC staining results revealed that the treatment with the two inhibitors reversed the rhFGF21-induced infarct volume reduction (Fig. 4d, e). These data suggest that rhFGF21 inhibits neuronal apoptosis by activating the PI3K/Akt pathway via FGFR1/β-klotho, thus mitigating brain damage in neonatal rats following HI.

3.4. rhFGF21 has neuroprotective effects that can be inhibited by PD173074 and LY294002

Subsequently, we conducted HE staining (Fig. 5a–d) and Nissl staining (Fig. 5e–h) to observe neuron the morphology and Nissl body integrity 7 d post-HI injury (P 14). These histological stains were performed to evaluate the hypoxic-ischemic cell damage by counting the cell numbers in the injured hemisphere. In the DMSO-treated sham group, the neurons in the cortex, hippocampal CA3 region and dentate gyrus (DG) were neatly arranged with distinct shapes. The Nissl bodies were large and numerous around the nuclei. However, after the HI injury, the neurons were disordered with pyknotic nuclei, and even the absence of neurons was observed. Few Nissl bodies were observed in the injured brain region. After the rhFGF21 treatment, the numbers of neurons and Nissl bodies increased. In contrast, the pretreatment with PD173074 or LY294002 partially inhibited the rhFGF21-induced neuronal density increases and morphological recovery.

Microtubule-associated protein-2 (MAP-2) is a specific structural protein expressed mainly in neuronal dendrites that stabilizes microtubules against depolymerization (Chen et al., 2017b). A western blot analysis and immunohistochemical staining of MAP-2 were performed 7 d post-HI insult. Compared with the DMSO-treated HI group, the rhFGF21-treated group showed an obvious increase in the expression of MAP-2. This increase in MAP-2 expression was inhibited by the treatment with the two inhibitors (Fig. 6a, b). The immunohistochemical staining revealed that compared with the DMSO treatment, the rhFGF21 treatment drastically reduced the loss of ipsilateral hemisphere MAP-2 positive staining (19.87 ± 4.81% vs. 44.2 ± 5.97%, $P < .05$). PD173074 and LY294002 suppressed the protective effect of rhFGF21 (Fig. 6c, d). Furthermore, the results of the immunohistochemical quantitative analysis in the cortex and hippocampal CA3 region were consistent with those of the western blot analysis (Fig. 6e–g). Taken together, these data show that rhFGF21 had

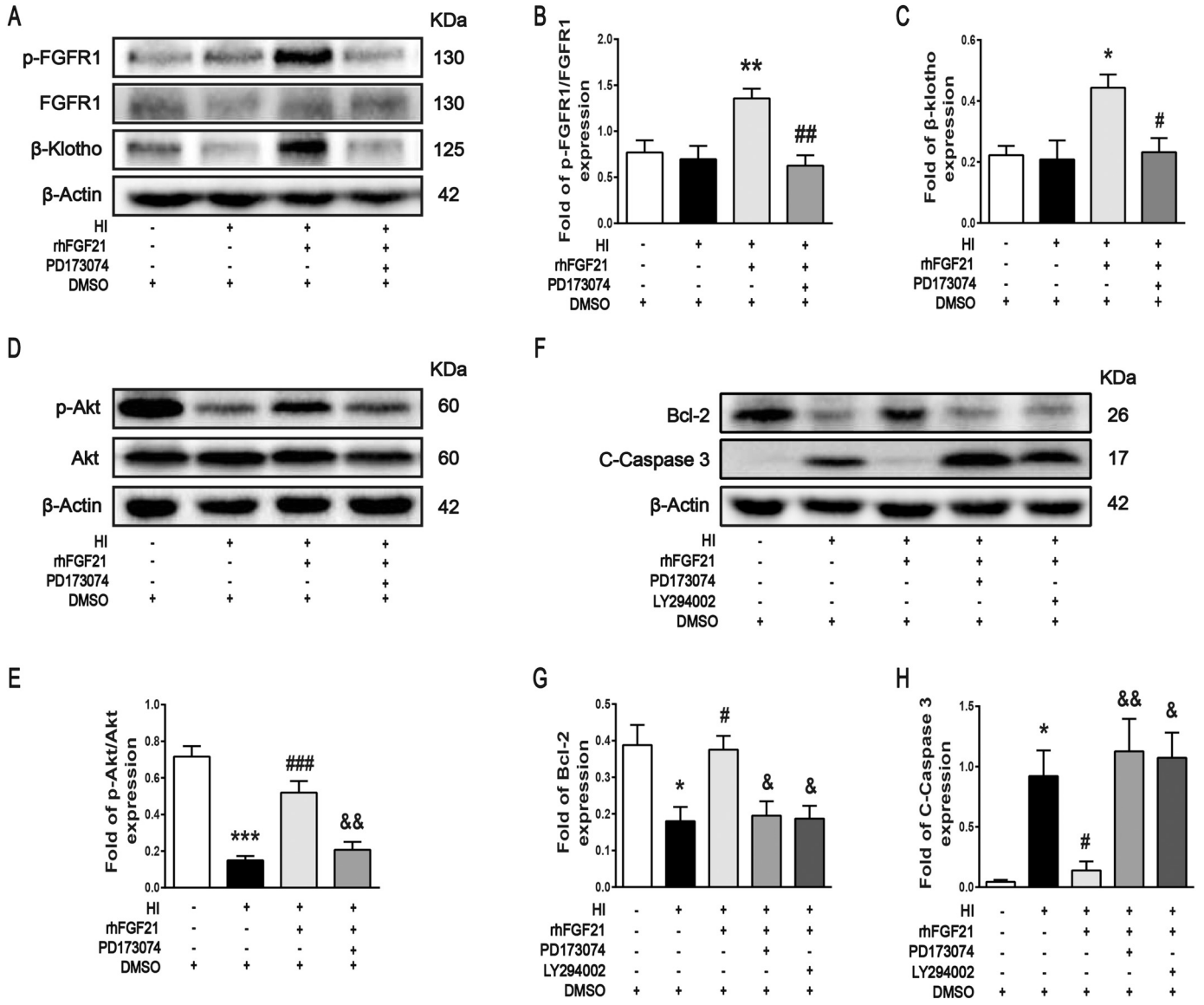

Fig. 3. rhFGF21 treatment mitigated HI-induced neuronal apoptosis by increasing p-Akt expression via FGFR1/β-klotho. (a) Representative western blot images of p-FGFR1, FGFR1 and β-klotho 4 h post-HI. (b, c) Effects of rhFGF21 and the FGFR1 inhibitor PD173074 on p-FGFR1/FGFR1 and β-klotho expression according to the western blot analysis data quantification. $^{*}P < .05$ and $^{**}P < .01$ vs. the HI + DMSO group; $^{\#}P < .05$ and $^{\#\#}P < .01$ vs. the HI + rhFGF21 + DMSO group. (d) Representative western blot images of p-Akt and Akt 24 h post-HI. (e) Effects of rhFGF21 and PD173074 on p-Akt/Akt according to the western blot analysis data quantification. (f) Representative images of Bcl-2 and cleaved caspase 3 at 3 d post-HI. (g-h) Effects of PD173074 and the PI3K inhibitor LY294002 on Bcl-2 (g) and cleaved caspase 3 (h) according to the western blot data analysis quantification. $^{*}P < .05$ and $^{***}P < .001$ vs. the sham + DMSO group; $^{\#}P < .05$ and $^{\#\#\#}P < .001$ vs. the HI + DMSO group; $^{\&}P < .05$ and $^{\&\&}P < .01$ vs. the HI + rhFGF21 + DMSO group. The values represent the mean ± SEM, n = 6.

neuroprotective effects and stabilized microtubule function after HI brain injury.

3.5. rhFGF21 ameliorates motor and cognitive functioning in HI-injured rats

To assess the influence of rhFGF21 on HI-induced motor deficits, the rotarod test was applied 21 d after the HI insult (P 28). The endurance times in the DMSO-treated HI group were significantly lower than those in the DMSO-treated sham group (88.38 ± 12.06 s vs. 144.90 ± 3.17 s, $P < .001$). After the rhFGF21 treatment, the endurance time increased to 128.10 ± 7.45 s. As expected, the PD173074 or LY294002 coadministration with rhFGF21 partially reversed the lengthened endurance times (Fig. 7a). Altogether, these data show that rhFGF21 could alleviate motor disability in rats after HI injury.

We used the Morris water maze to evaluate the learning and memory functioning of the rats in the different groups. (a) The spatial acquisition test: data indicated that the learning ability of the rats decreased following HI, which manifested as prolonged mean escape latencies (38.88 ± 1.16 s vs. 26.13 ± 2.26 s, $P < .01$). The rats in the HI + rhFGF21 + DMSO group spent less time finding the hidden platform than the HI-injured rats ($P < .05$). However, both PD173074 and LY294002 reversed the effect of rhFGF21 (Fig. 7b, c). (b) In the reference memory test, 24 h after the last training, the platform was withdrawn, and we recorded the frequency of crossings at the original platform location to study the spatial memory of the rats. The rats in the HI + rhFGF21 + DMSO group had a higher crossing frequency than the rats in the DMSO-treated HI group, and these effects could be lessened by PD173074 and LY294002 (Fig. 7d, e). These data show that rhFGF21 ameliorated motor and cognitive functioning in rats post-HI.

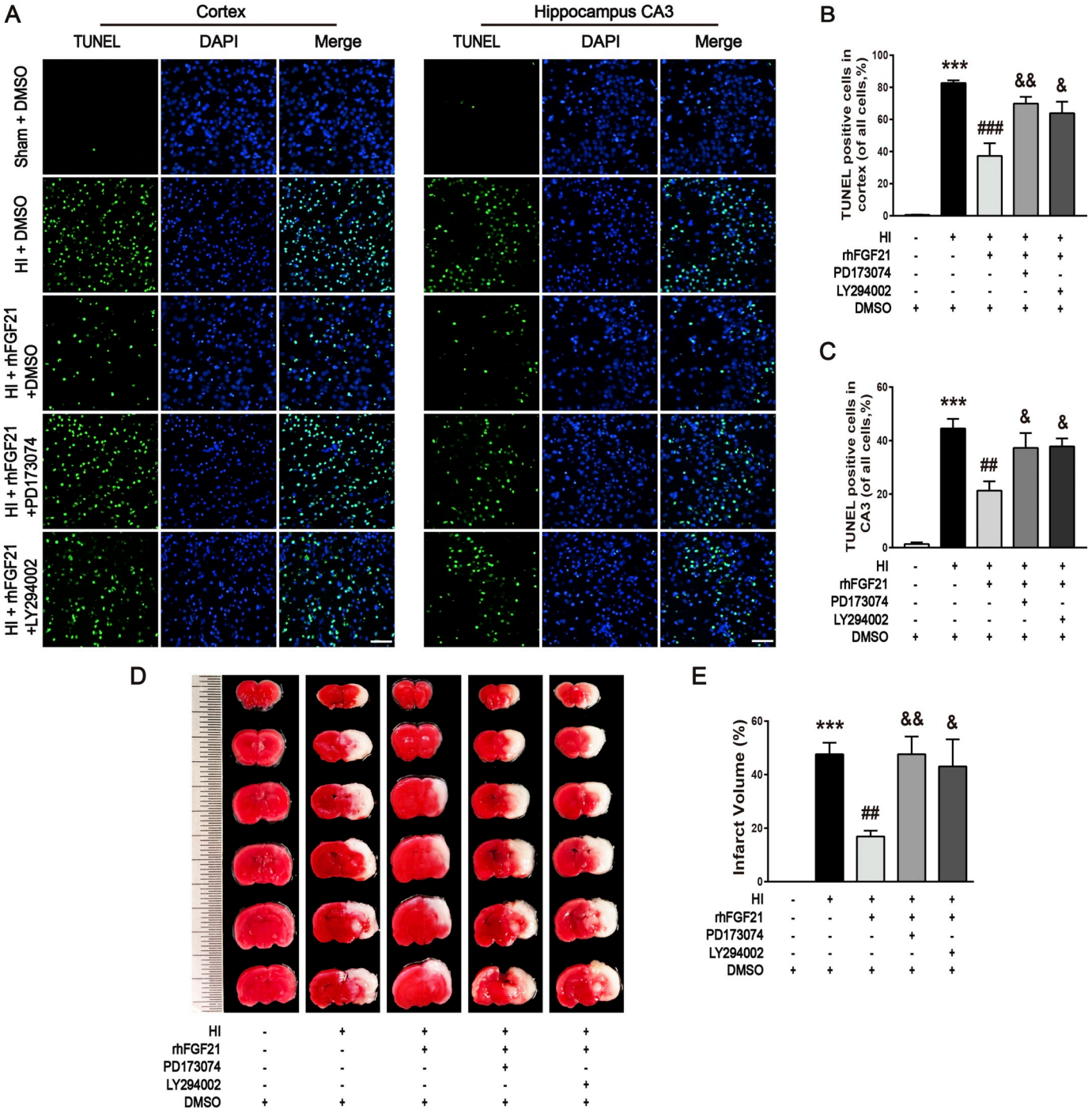

Fig. 4. The FGFR1 inhibitor PD173074 and the PI3K inhibitor LY294002 reversed the anti-apoptotic effect of rhFGF21 and increased the brain infarct volume. (a) Representative TUNEL-stained (*green*) and DAPI-stained (*blue*) brain sections of the cortex and hippocampus 3 d after HI. (b, c) Quantitative analysis of the percentage of TUNEL-positive cells in the cortex (b) and hippocampal CA3 region (c). (d)Representative photographs of TTC-stained coronal brain sections 3 d after HI. (e) Quantitative analysis of the brain infarct volume. $^{***}P < .001$ vs. the sham + DMSO group; $^{\#\#}P < .01$ and $^{\#\#\#}P < .001$ vs. the HI + DMSO group; $^{\&}P < .05$ and $^{\&\&}P < .01$ vs. the HI + rhFGF21 + DMSO group. The values represent the mean ± SEM, n = 6. Scale bar = 50 μm. (For interpretation of the references to colour in this figure legend, the reader is referred to the web version of this article.)

3.6. rhFGF21 alleviates OGD-induced primary cortical neuronal death by activating the PI3K/Akt pathway via FGFR1/β-klotho

To verify the above mentioned in vivo mechanisms, we generated a neuronal in vitro OGD model. This OGD model has been widely used to imitate HI-induced neuron damage (Zhao et al., 2015). Primary cortical neurons were exposed to OGD for 2 h, and different doses of rhFGF21 (0, 5, 10, and 50 nM) were administered post-OGD. After reoxygenation for 24 h, we used CCK-8 assays to test the neuronal viability. The results illustrated that different doses of rhFGF21 had no influence on neuronal viability (Fig. 8a). OGD reduced the number of live neurons to approximately 66%. Both 10 nM and 50 nM rhFGF21 could protect neurons from the OGD insult (Fig. 8b). These results show that rhFGF21 alleviated the primary neuronal damage after OGD, and 10 nM was considered the best concentration.

To prove that rhFGF21 activated the FGFR1/β-klotho receptor

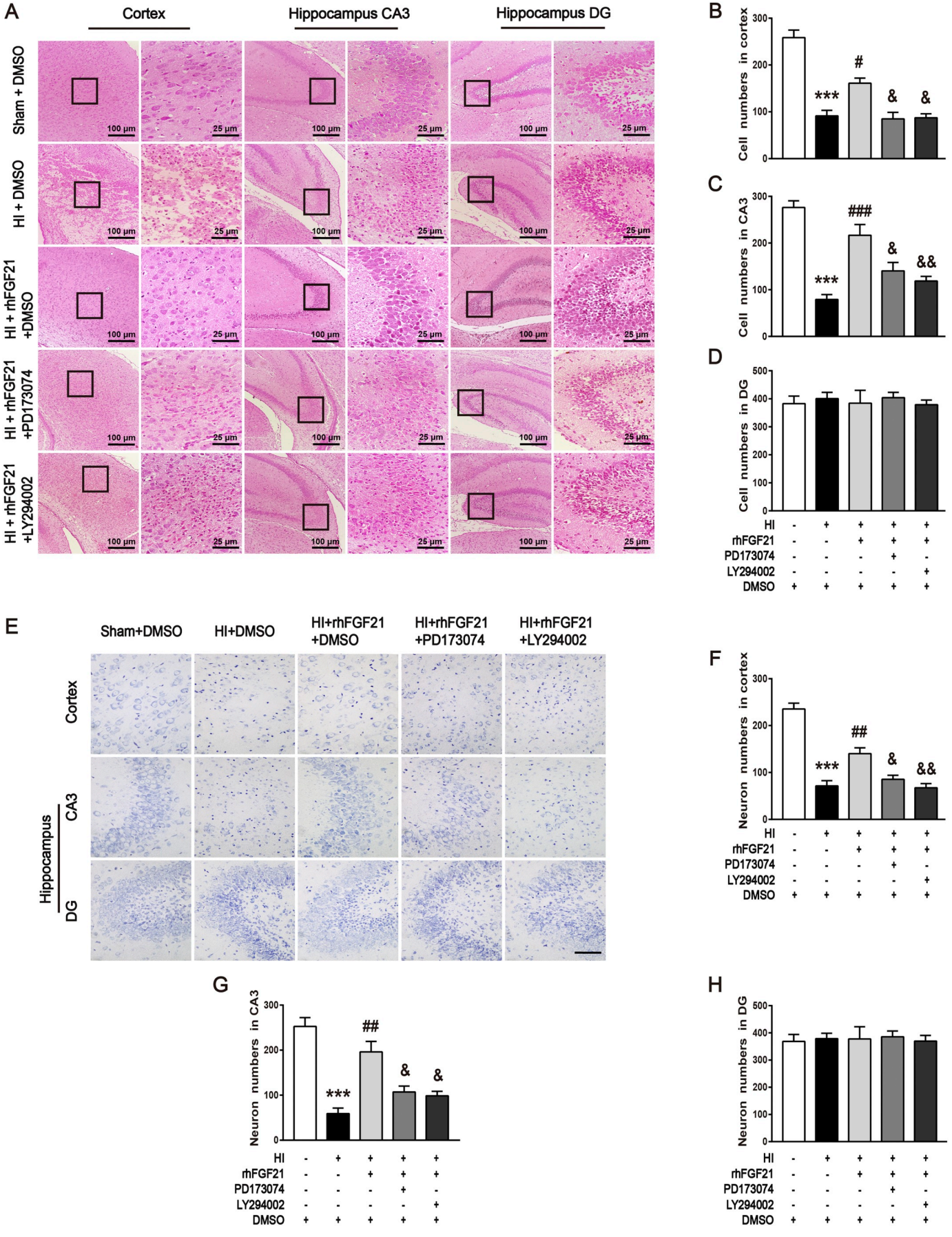

(caption on next page)

Fig. 5. rhFGF21 treatment ameliorated the tissue structure and increased the neuronal density after HI injury. (a) Representative images of HE staining in the cortex, hippocampal CA3 and DG region 7 d post-HI. The columns on the right show magnified images of the black boxes in the left column. Scale bars = 25 μm, 100 μm. (b–d) Number of cells in the cortex, hippocampal CA3 and DG region in each group (e) Representative images of Nissl staining in the cortex and hippocampus (CA3 and DG) in the injured ipsilateral brain 7 d post-HI. Scale bar = 25 μm. (f–h) Number of neurons in the cortex, hippocampal CA3 and DG region in each group. $^{***}P < .001$ vs. the sham + DMSO group; $^{\#}P < .05$, $^{\#\#}P < .01$ and $^{\#\#\#}P < .001$ vs. the HI + DMSO group; $^{\&}P < .05$ and $^{\&\&}P < .01$ vs. the HI + rhFGF21 + DMSO group. The values represent the mean ± SEM, n = 6.

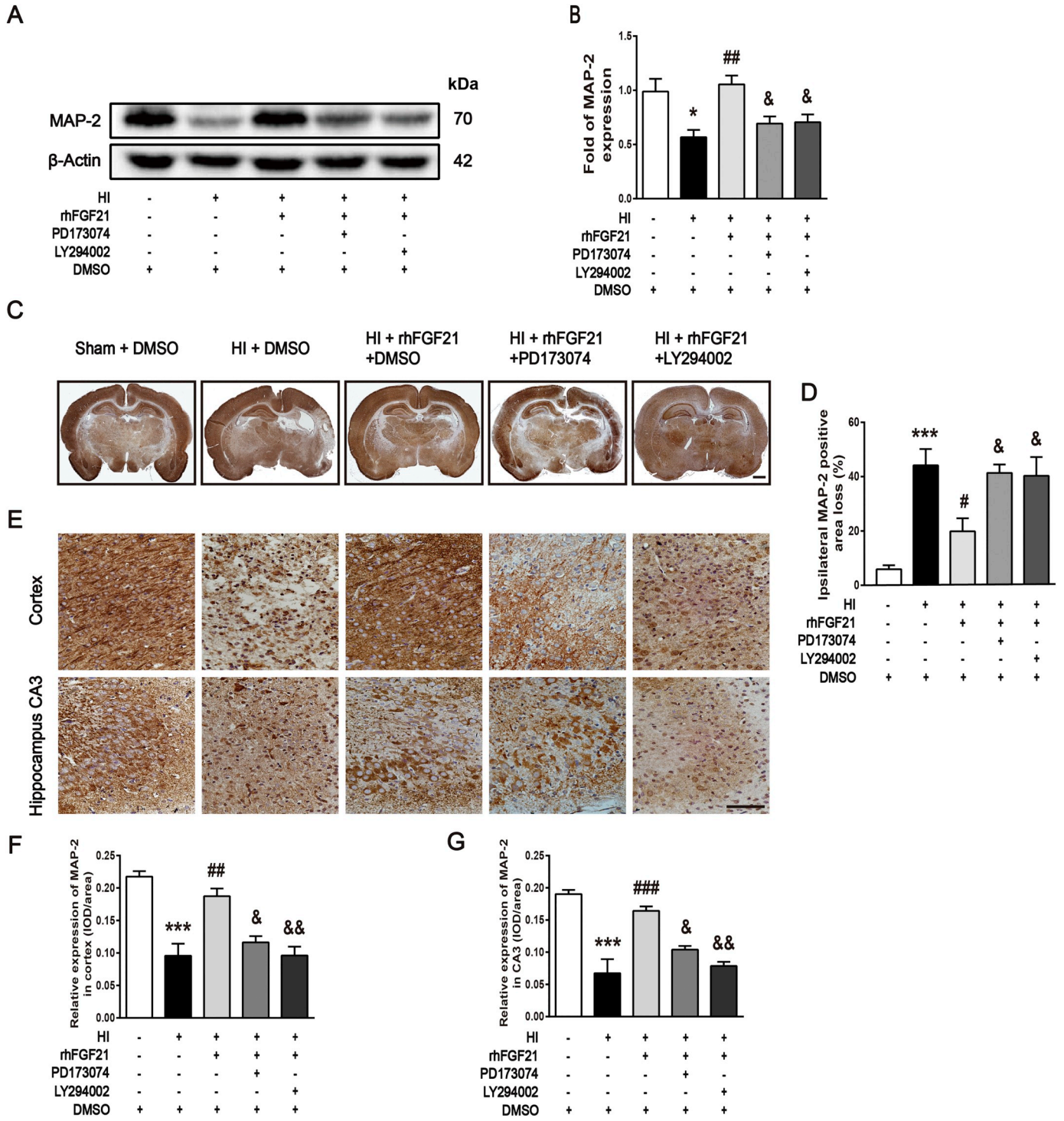

Fig. 6. rhFGF21 treatment stabilized microtubule function in rats post-HI injury. (a,b) Representative western blot images and quantification of MAP-2 expression 7 d post-HI. (c) Representative images of immunohistochemical staining of MAP-2 7 d post-HI. Scale bar = 1 mm. (d) Quantification of the percentage of the injured ipsilateral MAP-2-positive area loss. (e) Magnification of the cortex and hippocampal CA3 region in the images shown in (c). Scale bar = 25 μm. (f, g) Quantification of the average IOD of MAP-2 positive staining in the cortex and hippocampal CA3 region. $^{*}P < .05$ and $^{***}P < .001$ vs. the sham + DMSO group; $^{\#}P < .05$, $^{\#\#}P < .01$ and $^{\#\#\#}P < .001$ vs. the HI + DMSO group; $^{\&}P < .05$ and $^{\&\&}P < .01$ vs. the HI + rhFGF21 + DMSO group. The values represent the mean ± SEM, n = 6. IOD/area: Integrated optical density per stained area.

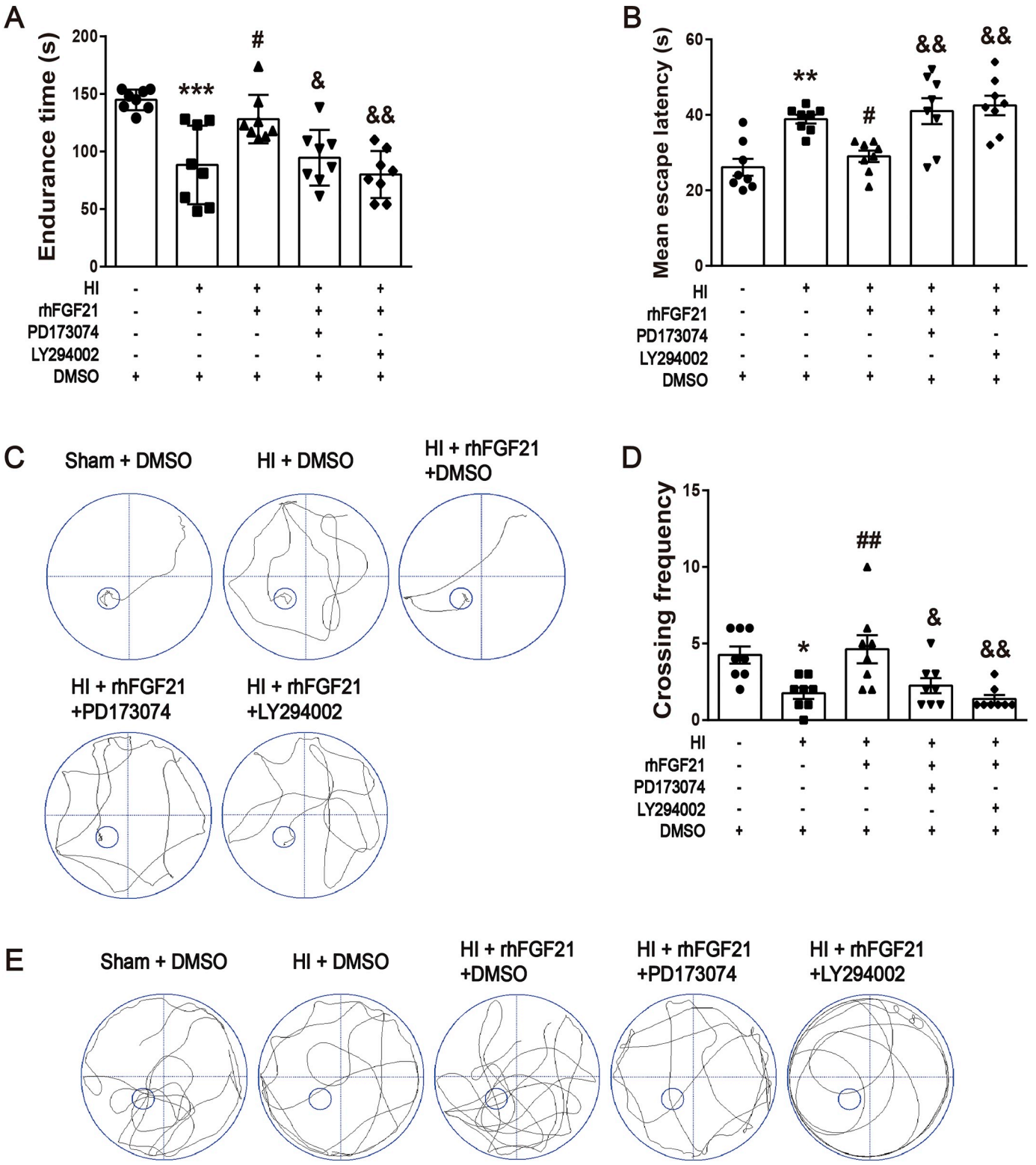

Fig. 7. rhFGF21 treatment ameliorated motor, learning and memory functions in HI-injured rats. (a) Rotarod performance tests for the motor coordination evaluation were performed 21 d after the HI insult. (b) MWM tests were conducted 21 d after the HI insult. The spatial acquisition tests for the learning ability evaluation lasted for 5 d. (c) Representative images of swim routes to locate the platform in the rats in the different groups. (d) Reference memory tests were used to assess spatial memory function. Quantification of the crossing frequency at the original platform location in 60 s. (e) Representative images of swim routes of rats after withdrawing the platform. $^{*}P < .05$, $^{**}P < .01$, and $^{***}P < .001$ vs. the sham + DMSO group; $^{\#}P < .05$ and $^{\#\#}P < .01$ vs. the HI + DMSO group; $^{\&}P < .05$ and $^{\&\&}P < .01$ vs. the HI + rhFGF21 + DMSO group. The values represent the mean ± SEM, n = 8.

complex in primary neurons, western blotting and immunofluorescence staining were conducted 1 h after the drug administration. The western blot analysis results were similar to those of the in vivo experiment. One hour after the rhFGF21 treatment, the p-FGFR1 and β-klotho expression levels were higher than those in the OGD group, and these effects were inhibited by PD173074 (10 nM) (Fig. 8c–e). The double

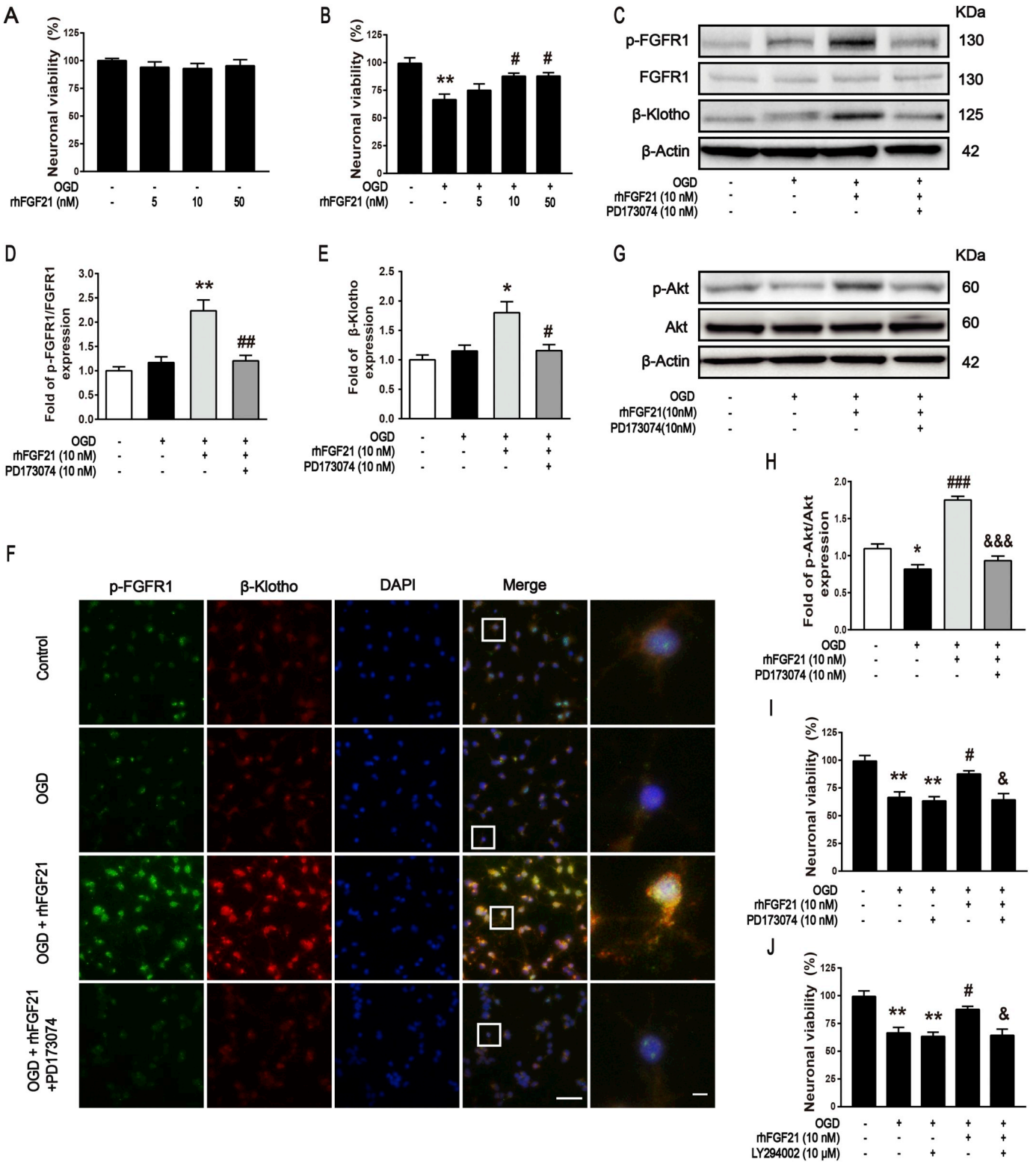

Fig. 8. rhFGF21 alleviated primary cortical neuronal death after OGD by activating the PI3K/Akt pathway via FGFR1/β-klotho. (a) Neuronal viability after the administration of different doses of rhFGF21 under normal conditions. (b) Neuronal viability after reoxygenation for 24 h after OGD for 2 h. $^{**}P < .01$ vs. the control group; $^{\#}P < .05$ vs. the OGD group. (c) Representative western blot images of p-FGFR1, FGFR1 and β-klotho 1 h post-OGD insult. (d, e) Effects of rhFGF21 (10 nM) and the FGFR1 inhibitor PD173074 (10 nM) on p-FGFR1/FGFR1 and β-klotho expression according to the western blot analysis data quantification. $^{*}P < .05$ and $^{**}P < .01$ vs. the OGD group; $^{\#}P < .05$ and $^{\#\#}P < .01$ vs. the OGD + rhFGF21 group. (f) Representative immunofluorescence costaining images of p-FGFR1 (*green*) and β-klotho (*red*) 1 h post-OGD insult. Scale bar = 50 μm. The columns on the right show magnified images of the white boxes. Scale bar = 5 μm. (g, h) Representative western blot images and quantification of p-Akt/Akt. (i, j) Effects of the FGFR1 inhibitor PD173074 (10 nM) and the PI3K inhibitor LY294002 (10 μM) on neuronal viability 24 h after OGD for 2 h. $^{*}P < .05$ and $^{**}P < .01$ vs. the control group; $^{\#}P < .05$ and$^{\#\#\#}P < .001$ vs. the OGD group; $^{\&}P < .05$ and$^{\&\&\&}P < .001$ vs. the OGD + rhFGF21 group. The values represent the mean ± SEM, n = 4. (For interpretation of the references to colour in this figure legend, the reader is referred to the web version of this article.)

immunofluorescence staining of p-FGFR1 and β-klotho supported the western blot analysis results (Fig. 8f). In addition, we found that PD173074 alone had no cytotoxicity, but its coadministration with rhFGF21 inhibited the rhFGF21-induced increase in neuronal viability (Fig. 8i). Subsequently, we measured the expression of p-Akt and Akt through western blotting. The p-Akt/Akt ratio was decreased 1 h after OGD, and this ratio was obviously increased after the rhFGF21 treatment. PD173074 reversed this change in p-Akt (Fig. 8g, h). The CCK-8 results indicated that LY294002 (10 μM) inhibited the protective effect of rhFGF21 in neurons post-OGD without inducing cytotoxicity (Fig. 8j). Thus, rhFGF21 inhibited OGD-induced neuronal death in vitro by activating the PI3K/Akt pathway via FGFR1/β-klotho.

3.7. FGF21 protects primary cortical neurons from OGD injury by attenuating neuronal apoptosis

To demonstrate that rhFGF21 prevented OGD-induced primary cortical neuronal apoptosis, we detected the expression of apoptosis-related proteins (cleaved caspase 3 and Bcl-2) and performed TUNEL staining 24 h after OGD. PD173074 and LY294002 were also applied to further evaluate this effect. After OGD/R for 24 h, Bcl-2 expression decreased, and cleaved caspase 3 expression increased. In contrast, the rhFGF21 treatment attenuated neuronal apoptosis after OGD. The anti-apoptotic effect of rhFGF21 was inhibited by PD173074 and LY294002 (Fig. 9a–c). The TUNEL staining results showed that the rhFGF21 treatment significantly decreased the number of TUNEL-positive cells from 46.25 ± 3.47% to 27.75 ± 3.75% ($P < .05$) (Fig. 9d, e). This protective effect was partially reversed by PD173074 and LY294002.

We also measured the expression level of MAP-2 by western blotting and immunofluorescence staining after OGD/R 24 h. The western blot analysis data showed that the expression of MAP-2 decreased after OGD/R for 24 h. However, MAP-2 expression was increased after the rhFGF21 treatment, and both PD173074 and LY294002 partially suppressed the expression of MAP-2 (Fig. 9f, g). The immunofluorescence staining results were consistent with the western blotting results. The MAP-2-positive primary cortical neurons were tightly connected, and neuritis were interwoven into nets under the control conditions. OGD reduced the number of MAP-2-positive neurons, and a portion of the neurites were fractured. The rhFGF21 treatment mitigated the OGD-induced neuronal destruction and increased the number of MAP-2-positive cells. The neuroprotective effect of rhFGF21 was partially reversed by PD173074 and LY294002 (Fig. 9h). These results indicate that rhFGF21 inhibits neuronal apoptosis to protect primary cortical neurons from OGD injury.

4. Discussion

Perinatal asphyxia often results in neonatal HI brain injury, which is associated with high mortality and severe long-term neurological deficits in newborns (Yıldız et al., 2016; Zalewska et al., 2015). Recent clinical and animal studies indicate that therapeutic hypothermia alone provides limited neuroprotection because hypothermia is unable to promote tissue repair, which is needed for neurodevelopment (Zalewska et al., 2015). Therefore, new synergistic therapies are needed to improve the outcome of hypothermia in patients with neonatal HI brain injury.

FGF21 is a recently discovered metabolic regulator that facilitates glucose and lipid metabolism. Animal studies suggest that FGF21 has potential therapeutic effects on obesity and diabetes (Kharitonenkov, 2009; Kharitonenkov et al., 2007; Woo et al., 2013). However, its function and mechanism in brain injury remain unclear. Evidence has shown that FGF21 plays important roles in circadian behavior, neuroprotection and cognition (Sa-nguanmoo et al., 2016a). Here, we explored the protective effects of FGF21 in neonatal rats following HI injury and investigated the possible underlying mechanism. In the present study, we demonstrated that rhFGF21 exerted both short-term and long-term neuroprotective functions. We found that rhFGF21 treatment reduced the brain infarct volume and brain atrophy extent, improved body weight, inhibited neuronal apoptosis and ameliorated the histological structure in the short-term. Furthermore, we revealed that rhFGF21 could ameliorate motor, learning and spatial memory functioning in the long-term. Specifically, all these protective functions could be partially reversed by additional treatment with PD173074 or LY294002. Using an in vitro OGD model of primary cortical neurons, we revealed that the rhFGF21 treatment promoted neuronal survival and suppressed neuronal apoptosis. After using both rhFGF21 and PD173074 or LY294002, OGD-induced cell death was increased compared with that following the rhFGF21 treatment alone. Importantly, by performing both in vivo and in vitro experiments, we demonstrated that rhFGF21 inhibits neuronal apoptosis by activating the PI3K/Akt signaling pathway via forming an FGF21/FGFR1/β-klotho complex. Thus, our results suggest that rhFGF21 may be beneficial to the recovery of neonatal HI brain injury.

The immature brain is relatively more resistant to hypoxia alone than the adult brain due to its strong protective mechanisms, such as its collateral circulation compensative capacity. Neonatal brain injury can occur over several days only when hypoxia is combined with an ischemic event (Johnston et al., 2001; Rocha-Ferreira and Hristova, 2016). The laser speckle contrast imaging data revealed that our HI model could efficiently decrease cortical blood perfusion 24 h after HI. Neurons are extremely vulnerable to even brief periods of ischemia because they lack the necessary enzyme for effective glycolysis (Li et al., 2017). After blocking blood flow, anaerobic lactate production rapidly leads to acidosis, followed by neuronal death (Mungai et al., 2011). HI injury leads to selective damage in different brain regions but not uniform or global brain injury (Johnston et al., 2001). As shown by the TTC data, HI resulted in an approximately 47% brain infarct volume 3 d after injury, and 1.5 mg/kg rhFGF21 efficiently reduced this infarct volume. In addition, we demonstrated that the rhFGF21 treatment alleviated brain atrophy and improved the body weight of rat pups after HI injury. These results confirm that rhFGF21 has short-term protective effects that can reduce cerebral infarction and improve the overall health level.

To explore the potential protective mechanism of rhFGF21 in neonatal rats post-HI, we measured the expression of p-FGFR1/FGFR1 and β-klotho. FGFR1 is the primary receptor of FGF21 that mediates its activity; β-klotho is an essential coreceptor for FGF21 activity, and cells are unable to respond to FGF21 without β-klotho (Sa-nguanmoo et al., 2016a). In the current study, we found that rhFGF21 increased the p-FGFR1/FGFR1 and β-klotho levels both in vivo and in vitro and that this effect could be inhibited by the FGFR1 inhibitor PD173074. However, the total FGFR1 levels remained unchanged. These animal findings are consistent with the findings of our previous study in post-TBI mice (Chen et al., 2018b). However, after the rhFGF21 treatment, the expression level of β-klotho differed from that in some published reports of obese rodent models (Sa-Nguanmoo et al., 2016b; Wang et al., 2018c). This inconsistency may be attributed to the different models or different sampling sites and time points.

Increasing evidence suggests that the activation of PI3K/Akt and its downstream pathways inhibits neuronal apoptosis (Tu et al., 2018), mediates axonal injury (Xiong et al., 2012), and improves cellular survival (Zhang et al., 2015) in models of HI brain damage. Wang et al. (2018c) proved that rFGF21 plays a vital role in mediating Akt/GSK-3β signaling in the hippocampus of an obese mouse model. Luan et al. (2018) reported that SC79, which is a small molecule Akt activator, reduced the infarct volume of ischemic brains and improved the neurological functioning of rats after cerebral ischemia/reperfusion injury. PI3K/Akt signaling pathway activation in astrocytes reportedly associated with neuronal protection under OGD/R conditions (Liu et al., 2017). Consistent with the results of a previous study (Xiong et al., 2012), we found that the expression of p-Akt, but not total Akt, was decreased 24 h after HI. This decrease in p-Akt was also observed in

primary neurons 1 h after OGD. However, the rhFGF21 treatment increased the level of p-Akt both in vivo and in vitro, confirming our hypothesis.

Compared with the adult brain, different mechanisms of HI injury are activated in the immature brain; through these mechanisms, apoptosis is several-fold more pronounced in immature animal brains than in juvenile and adult brains (Semple et al., 2013; Zhu et al., 2005). Therefore, reducing neuronal apoptosis and promoting neuronal

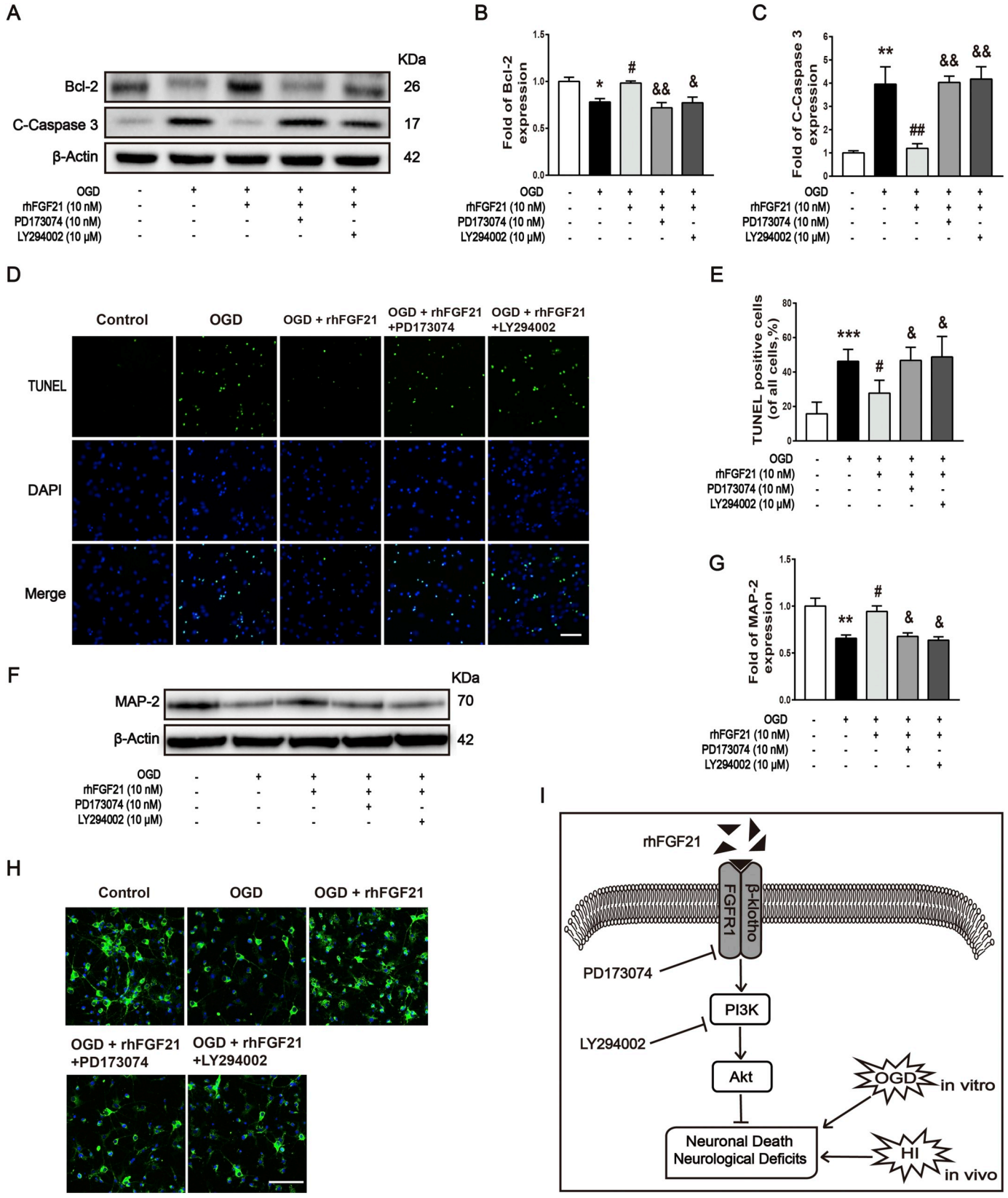

(caption on next page)

Fig. 9. rhFGF21 inhibited primary cortical neuronal apoptosis after OGD/R for 24 h, which was reversed by PD173074 and LY294002. (a–c) Representative western blot images and quantification of Bcl-2 and cleaved caspase 3 24 h post-OGD injury. (d) Representative TUNEL-stained (*green*) and DAPI-stained (*blue*) primary cortical neurons 24 h after HI. (e) Quantification of the percentage of TUNEL-positive neurons. (f, g) Representative western blot image and quantification of MAP-2 24 h post-OGD. (h) Representative immunofluorescence images of MAP-2 (*green*) 24 h post-OGD insult. $^{*}P < .05$, $^{**}P < .01$, and $^{***}P < .001$ vs. the control group; $^{\#}P < .05$ and $^{\#\#}P < .01$ vs. the OGD group; $^{\&}P < .05$ and $^{\&\&}P < .01$ vs. the OGD + rhFGF21 group. The values represent the mean ± SEM, n = 4. Scale bar = 50 μm. (i) Proposed mechanism underlying the rhFGF21-mediated neuroprotective effects after neonatal HI brain injury. Exogenous rhFGF21 combines with FGFR1 and β-Klotho at the neuronal cytomembrane to form a stable FGF21/FGFR1/β-klotho complex. Then, activated downstream PI3K/Akt signaling pathways play a role in reducing neuronal death and promoting neurofunctional recovery after OGD or HI insult. The FGFR1 inhibitor PD173074 or the PI3K inhibitor LY294002 was combined with rhFGF21 to test the suggested signaling pathways. (For interpretation of the references to colour in this figure legend, the reader is referred to the web version of this article.)

survival are important strategies for treating brain injury associated with HI. Nakajima et al. (2000) reported that > 50% of degenerating cells in the cerebral cortex and basal ganglia of neonatal rats following HI are apoptotic, and the number of apoptotic cells in these regions remains high for more than a week after HI. The caspases are known to be synthesized as inactive pro-enzymes and are activated by proteolytic cleavage (Siklos et al., 2015). Cleaved caspase 3 is released at high levels specifically by the activation of HI (Yıldız et al., 2016). Previous studies have demonstrated that FGF21 protects cardiomyocytes from apoptosis (Liu et al., 2013; Wu et al., 2015). In addition, the anti-apoptotic function of FGF21 in the brain has been demonstrated in high-fat diet-induced obesity in rats (Sa-Nguanmoo et al., 2016b). Consistent with these findings, we illustrated that apoptosis was activated in the cortex and hippocampus 3 d after HI. We also demonstrated that rhFGF21 mitigated neuronal apoptosis and promoted cell survival to protect against HI insult in neonatal rats. PD173074 and LY294002 reversed the anti-apoptotic function of rhFGF21. Taken together, we illustrated that FGF21 inhibits neuronal apoptosis following HI and OGD by forming an FGF21/FGFR1/β-klotho complex to activate the PI3K/Akt signaling pathway.

Approximately 25% of survivors of neonatal HI brain injury have long-term neurological deficits, such as irreversible motor function and learning disorders (Lai and Yang, 2011). Therefore, in this study, we focused on the recovery of motor and learning functioning after HI injury. Skoff et al. (2007) reported that regrowing axons cannot innervate their normal targets because of the physical boundaries of the lesion and the abnormal cell types in the injured hemisphere, which may account for the existence of long-term functional deficits. Previous studies have shown that FGF21 administration improves cognitive function in obese insulin-resistant rats (Sa-Nguanmoo et al., 2016b), obese mice (Wang et al., 2018c) and D-galactose-induced aged mice (Yu et al., 2015). Consistent with these findings, our Morris water maze results showed that rhFGF21 improved the learning and memorization abilities of the HI-insulted rats. Furthermore, we proved that rhFGF21 contributes to restoring motor coordination according to the rotarod test results. FGF21 has been reported to inhibit cognitive function decline in obese insulin-resistant rats mainly by restoring synaptic plasticity, dendritic spine density, brain mitochondrial function, and cell apoptosis (Sa-Nguanmoo et al., 2016b). Wang et al. (2018c) revealed that FGF21 promotes hippocampal neurogenesis to attenuate high-fat diet-induced cognitive impairment. In addition to the inhibitory effect of rhFGF21 on cortical and hippocampal neuronal apoptosis, other possible mechanisms of the recovery of motor and cognitive functioning need to be explored further.

FGF21-associated drugs have recently been developed for the treatment of diabetes, and some compounds have reached the stage of clinical trials (Gaich et al., 2013). Although our experimental results are translationally significant, there are still some limitations. First, the protection mechanism of FGF21 is not comprehensive enough in our research. As previously mentioned, in addition to the PI3K/Akt pathway, FGF21 activates other multiple downstream signaling pathways, such as the RAS-RAF-MAPK, STAT, and PLCγ pathways (Itoh and Ornitz, 2011). In addition, the anti-inflammatory effect of FGF21 has been recently shown in a diabetic model (Wang et al., 2018b). Wang et al. (2018c) found that FGF21 suppresses microglia activation and pro-inflammatory cytokine expression in the hippocampus, cortex and hypothalamus of obese mice. Therefore, further research is needed to explore the neuroprotective mechanisms of FGF21 more extensively, especially the aspect of neuroinflammation. Second, although our experiments showed that FGF21 activated the FGFR1/β-klotho receptor complex on cultured neurons in vitro, we did not define the specific brain regions and cell types where FGF21/FGFR1/β-klotho activation occurred in vivo. FGF21-induced receptor activation in the brain is worthy of future investigation. Furthermore, therapeutic hypothermia has been regarded as the only reliable standard therapy for neonatal encephalopathy but is unable to promote tissue repair alone. Combined with our findings in the current study that rhFGF21 performs a neuroprotective function after HI injury, in our future studies, it is necessary to explore the effects of combination therapy involving rhFGF21 and hypothermia in neonatal HI brain injury.

In conclusion, our current study demonstrated that an exogenous rhFGF21 treatment efficaciously reduced the infarct volume, promoted tissue morphological recovery, and ameliorated motor and learning disabilities in neonatal rats following HI brain injury. By performing both in vivo and in vitro experiments, we confirmed that exogenous rhFGF21 promoted neuronal survival and neurofunctional recovery after HI insult by forming the FGF21/FGFR1/β-klotho complex, which activated the PI3K/Akt signaling pathway (Fig. 9i). In conclusion, our results revealed that rhFGF21 may be a promising therapeutic agent for neonatal HI brain injury, and more detailed studies investigating its protective mechanism should be conducted.

Conflicts of interest

The authors have no conflicts of interest to declare.

Acknowledgments

This study was supported by grants from the National Natural Science Foundation of China (NO. 81771284 and 81771624), the Beijing Medical and Health Foundation (NO. B17137), and the Public Welfare Technology Application Research Foundation of Zhejiang Province (NO. 2017C33080).

Appendix A. Supplementary data

Supplementary data to this article can be found online at https://doi.org/10.1016/j.expneurol.2019.02.013.

References

Adams, A., Cheng, C., Coskun, T., Kharitonenkov, A., 2012. FGF21 requires βklotho to act in vivo. PLoS One 7, e49977. https://doi.org/10.1371/journal.pone.0049977.

Al-Macki, N., Miller, S., Hall, N., Shevell, M., 2009. The spectrum of abnormal neurologic outcomes subsequent to term intrapartum asphyxia. Pediatr. Neurol. 41, 399–405. https://doi.org/10.1016/j.pediatrneurol.2009.06.001.

Chen, H., Lin, W., Zhang, Y., Lin, L., Chen, J., Zeng, Y., Zheng, M., Zhuang, Z., Du, H., Chen, R., Liu, N., 2016. IL-10 promotes neurite outgrowth and synapse formation in cultured cortical neurons after the oxygen-glucose deprivation via JAK1/STAT3 pathway. Sci. Rep. 6, 30459. https://doi.org/10.1038/srep30459.

Chen, J., Du, H., Zhang, Y., Chen, H., Zheng, M., Lin, P., Lan, Q., Yuan, Q., Lai, Y., Pan, X., Chen, R., Liu, N., 2017a. Netrin-1 prevents rat primary cortical neurons from

apoptosis via the DCC/ERK pathway. Front. Cell. Neurosci. 11, 387. https://doi.org/10.3389/fncel.2017.00387.
Chen, J., Wang, Z., Zheng, Z., Chen, Y., Khor, S., Shi, K., He, Z., Wang, Q., Zhao, Y., Zhang, H., Li, X., Li, J., Yin, J., Wang, X., Xiao, J., 2017b. Neuron and microglia/macrophage-derived FGF10 activate neuronal FGFR2/PI3K/Akt signaling and inhibit microglia/macrophages TLR4/NF-kappaB -dependent neuroinflammation to improve functional recovery after spinal cord injury. Cell Death Dis. 8, e3090. https://doi.org/10.1038/cddis.2017.490.
Chen, D., Dixon, B.J., Doycheva, D.M., Li, B., Zhang, Y., Hu, Q., He, Y., Guo, Z., Nowrangi, D., Flores, J., Filippov, V., Zhang, J.H., Tang, J., 2018a. IRE1α inhibition decreased TXNIP/NLRP3 inflammasome activation through miR-17-5p after neonatal hypoxic–ischemic brain injury in rats. J. Neuroinflammation 15. https://doi.org/10.1186/s12974-018-1077-9.
Chen, J., Hu, J., Liu, H., Xiong, Y., Zou, Y., Huang, W., Shao, M., Wu, J., Yu, L., Wang, X., Wang, X., Lin, L., 2018b. FGF21 protects the blood–brain barrier by upregulating PPARγ via FGFR1/β-klotho after traumatic brain injury. J. Neurotrauma 35, 2091–2103. https://doi.org/10.1089/neu.2017.5271.
Cong, W.T., Ling, J., Tian, H.S., Ling, R., Wang, Y., Huang, B.B., Zhao, T., Duan, Y.M., Jin, L.T., Li, X.K., 2013. Proteomic study on the protective mechanism of fibroblast growth factor 21 to ischemia- reperfusion injury. Can. J. Physiol. Pharmacol. 91, 973–984. https://doi.org/10.1139/cjpp-2012-0441.
Douglas-Escobar, M., Weiss, M.D., 2015. Hypoxic-ischemic encephalopathy: a review for the clinician. JAMA Pediatr. 169, 397–403. https://doi.org/10.1001/jamapediatrics.2014.3269.
Fon Tacer, K., Bookout, A., Ding, X., Kurosu, H., John, G., Wang, L., Goetz, R., Mohammadi, M., Kuro-o, M., Mangelsdorf, D., Kliewer, S., 2010. Research resource: comprehensive expression atlas of the fibroblast growth factor system in adult mouse. Mol. Endocrinol. 24, 2050–2064. https://doi.org/10.1210/me.2010-0142.
Gaich, G., Chien, J., Fu, H., Glass, L., Deeg, M., Holland, W., Kharitonenkov, A., Bumol, T., Schilske, H., Moller, D., 2013. The effects of LY2405319, an FGF21 analog, in obese human subjects with type 2 diabetes. Cell Metab. 18, 333–340. https://doi.org/10.1016/j.cmet.2013.08.005.
Grandvuillemin, I., Garrigue, P., Ramdani, A., Boubred, F., Simeoni, U., Dignat-George, F., Sabatier, F., Guillet, B., 2017. Long-term recovery after endothelial Colony-forming cells or human umbilical cord blood cells Administration in a rat Model of neonatal hypoxic-ischemic encephalopathy. Stem Cells Transl. Med. 6, 1987–1996. https://doi.org/10.1002/sctm.17-0074.
Harding, B., Conception, K., Li, Y., Zhang, L., 2016. Glucocorticoids protect neonatal rat brain in model of hypoxic-ischemic encephalopathy (HIE). Int. J. Mol. Sci. 18. https://doi.org/10.3390/ijms18010017.
Hsuchou, H., Pan, W., Kastin, A., 2007. The fasting polypeptide FGF21 can enter brain from blood. Peptides 28, 2382–2386. https://doi.org/10.1016/j.peptides.2007.10.007.
Hu, S., Cao, S., Liu, J., 2017. Role of angiopoietin-2 in the cardioprotective effect of fibroblast growth factor 21 on ischemia/reperfusion-induced injury in H9c2 cardiomyocytes. Exp. Ther. Med. E 14, 771–779. https://doi.org/10.3892/etm.2017.4564.
Huang, B., Krafft, P.R., Ma, Q., Rolland, W.B., Caner, B., Lekic, T., Manaenko, A., Le, M., Tang, J., Zhang, J.H., 2012. Fibroblast growth factors preserve blood-brain barrier integrity through RhoA inhibition after intracerebral hemorrhage in mice. Neurobiol. Dis. 46, 204–214. https://doi.org/10.1016/j.nbd.2012.01.008.
Humeau-Heurtier, A., Mahé, G., Abraham, P., 2015. Microvascular blood flow monitoring with laser speckle contrast imaging using the generalized differences algorithm. Microvasc. Res. 98, 54–61. https://doi.org/10.1016/j.mvr.2014.12.003.
Itoh, N., Ornitz, D., 2011. Fibroblast growth factors: from molecular evolution to roles in development, metabolism and disease. J. Biochem. 149, 121–130. https://doi.org/10.1093/jb/mvq121.
Johnston, M., Trescher, W., Ishida, A., Nakajima, W., 2001. Neurobiology of hypoxic-ischemic injury in the developing brain. Pediatr. Res. 49, 735–741. https://doi.org/10.1203/00006450-200106000-00003.
Kharitonenkov, A., 2009. FGFs and metabolism. Curr. Opin. Pharmacol. 9, 805–810. https://doi.org/10.1016/j.coph.2009.07.001.
Kharitonenkov, A., Wroblewski, V., Koester, A., Chen, Y., Clutinger, C., Tigno, X., Hansen, B., Shanafelt, A., Etgen, G., 2007. The metabolic state of diabetic monkeys is regulated by fibroblast growth factor-21. Endocrinology 148, 774–781. https://doi.org/10.1210/en.2006-1168.
Kuroda, M., Muramatsu, R., Maedera, N., Koyama, Y., Hamaguchi, M., Fujimura, H., Yoshida, M., Konishi, M., Itoh, N., Mochizuki, H., Yamashita, T., 2017. Peripherally derived FGF21 promotes remyelination in the central nervous system. J. Clin. Invest. 127, 3496–3509. https://doi.org/10.1172/JCI94337.
Lai, M., Yang, S., 2011. Perinatal hypoxic-ischemic encephalopathy. J. Biomed. Biotechnol. 2011, 609813. https://doi.org/10.1155/2011/609813.
Li, L., Khatibi, N., Hu, Q., Yan, J., Chen, C., Han, J., Ma, D., Chen, Y., Zhou, C., 2012. Transmembrane protein 166 regulates autophagic and apoptotic activities following focal cerebral ischemic injury in rats. Exp. Neurol. 234, 181–190. https://doi.org/10.1016/j.expneurol.2011.12.038.
Li, D., Luo, L., Xu, M., Wu, J., Chen, L., Li, J., Liu, Z., Lu, G., Wang, Y., Qiao, L., 2017. AMPK activates FOXO3a and promotes neuronal apoptosis in the developing rat brain during the early phase after hypoxia-ischemia. Brain Res. Bull. 132, 1–9. https://doi.org/10.1016/j.brainresbull.2017.05.001.
Liu, S., Roberts, D., Kharitonenkov, A., Zhang, B., Hanson, S., Li, Y., Zhang, L., Wu, Y., 2013. Endocrine protection of ischemic myocardium by FGF21 from the liver and adipose tissue. Sci. Rep. 3, 2767. https://doi.org/10.1038/srep02767.
Liu, D., Zhang, M., Rong, X., Li, J., Wang, X., 2017. Potassium 2-(1-hydroxypentyl)-benzoate attenuates neuronal apoptosis in neuron-astrocyte co-culture system through neurotrophy and neuroinflammation pathway. Acta Pharm. Sin. B 7, 554–563. https://doi.org/10.1016/j.apsb.2017.06.006.
Luan, Q., Pan, L., He, D., Gong, X., Zhou, H., 2018. SC79, the AKT activator protects cerebral ischemia in a rat model of ischemia/reperfusion injury. Med. Sci. Monit. 24, 5391–5397. https://doi.org/10.12659/msm.910191.
Ma, Q., Zhang, L., 2018. C-type natriuretic peptide functions as an innate neuroprotectant in neonatal hypoxic-ischemic brain injury in mouse via natriuretic peptide receptor 2. Exp. Neurol. 304, 58–66. https://doi.org/10.1016/j.expneurol.2018.02.016.
Mäkelä, J., Tselykh, T., Maiorana, F., Eriksson, O., Do, H., Mudò, G., Korhonen, L., Belluardo, N., Lindholm, D., 2014. Fibroblast growth factor-21 enhances mitochondrial functions and increases the activity of PGC-1α in human dopaminergic neurons via Sirtuin-1. Springerplus 3, 2. https://doi.org/10.1186/2193-1801-3-2.
Mungai, P., Waypa, G., Jairaman, A., Prakriya, M., Dokic, D., Ball, M., Schumacker, P., 2011. Hypoxia triggers AMPK activation through reactive oxygen species-mediated activation of calcium release-activated calcium channels. Mol. Cell. Biol. 31, 3531–3545. https://doi.org/10.1128/MCB.05124-11.
Nakajima, W., Ishida, A., Lange, M.S., Gabrielson, K.L., Wilson, M.A., Martin, L.J., Blue, M.E., Johnston, M.V., 2000. Apoptosis has a prolonged role in the neurodegeneration after hypoxic ischemia in the newborn rat. J. Neurosci. 20, 7994–8004. https://doi.org/10.1523/JNEUROSCI.20-21-07994.2000.
Nakanishi, K., Sato, Y., Mizutani, Y., Ito, M., Hirakawa, A., Higashi, Y., 2017. Rat umbilical cord blood cells attenuate hypoxic-ischemic brain injury in neonatal rats. Sci. Rep. 7, 44111. https://doi.org/10.1038/srep44111.
Northington, F., Graham, E., Martin, L., 2005. Apoptosis in perinatal hypoxic-ischemic brain injury: how important is it and should it be inhibited? Brain Res. Brain Res. Rev. 50, 244–257. https://doi.org/10.1016/j.brainresrev.2005.07.003.
Pan, Y., Wang, B., Zheng, J., Xiong, R., Fan, Z., Ye, Y., Zhang, S., Li, Q., Gong, F., Wu, C., Lin, Z., Li, X., Pan, X., 2018. Pancreatic fibroblast growth factor 21 protects against type 2 diabetes in mice by promoting insulin expression and secretion in a PI3K/Akt signaling-dependent manner. J. Cell. Mol. Med. https://doi.org/10.1111/jcmm.14007.
Planavila, A., Redondo-Angulo, I., Ribas, F., Garrabou, G., Casademont, J., Giralt, M., Villarroya, F., 2015. Fibroblast growth factor 21 protects the heart from oxidative stress. Cardiovasc. Res. 106, 19–31. https://doi.org/10.1093/cvr/cvu263.
Rocha-Ferreira, E., Hristova, M., 2016. Plasticity in the neonatal brain following hypoxic-Ischaemic injury. Neural Plast. 2016, 4901014. https://doi.org/10.1155/2016/4901014.
Sa-nguanmoo, P., Chattipakorn, N., Chattipakorn, S.C., 2016a. Potential roles of fibroblast growth factor 21 in the brain. Metab. Brain Dis. 31, 239–248. https://doi.org/10.1007/s11011-015-9789-3.
Sa-Nguanmoo, P., Tanajak, P., Kerdphoo, S., Satjaritanun, P., Wang, X., Liang, G., Li, X., Jiang, C., Pratchayasakul, W., Chattipakorn, N., Chattipakorn, S., 2016b. FGF21 improves cognition by restored synaptic plasticity, dendritic spine density, brain mitochondrial function and cell apoptosis in obese-insulin resistant male rats. Horm. Behav. 85, 86–95. https://doi.org/10.1016/j.yhbeh.2016.08.006.
Semple, B.D., Blomgren, K., Gimlin, K., Ferriero, D.M., Noble-Haeusslein, L.J., 2013. Brain development in rodents and humans: identifying benchmarks of maturation and vulnerability to injury across species. Prog. Neurobiol. 106–107, 1–16. https://doi.org/10.1016/j.pneurobio.2013.04.001.
Siklos, M., BenAissa, M., Thatcher, G.R., 2015. Cysteine proteases as therapeutic targets: does selectivity matter? A systematic review of calpain and cathepsin inhibitors. Acta Pharm. Sin. B 5, 506–519. https://doi.org/10.1016/j.apsb.2015.08.001.
Silveira, R., Procianoy, R., 2015. Hypothermia therapy for newborns with hypoxic ischemic encephalopathy. J. Pediatr. 91, S78–S83. https://doi.org/10.1016/j.jped.2015.07.004.
Skoff, R., Bessert, D., Barks, J., Silverstein, F., 2007. Plasticity of neurons and glia following neonatal hypoxic-ischemic brain injury in rats. Neurochem. Res. 32, 331–342. https://doi.org/10.1007/s11064-006-9188-6.
Taniguchi, H., Andreasson, K., 2008. The hypoxic ischemic encephalopathy model of perinatal ischemia. J. Vis. Exp. https://doi.org/10.3791/955.
Tu, L., Wang, Y., Chen, D., Xiang, P., Shen, J., Li, Y., Wang, S., 2018. Protective effects of Notoginsenoside R1 via regulation of the PI3K-Akt-mTOR/JNK pathway in neonatal cerebral hypoxic-ischemic brain injury. Neurochem. Res. 43, 1210–1226. https://doi.org/10.1007/s11064-018-2538-3.
Wang, N., Li, J.Y., Li, S., Guo, X.C., Wu, T., Wang, W.F., Li, D.S., 2018a. Fibroblast growth factor 21 regulates foam cells formation and inflammatory response in ox-LDL-induced THP-1 macrophages. Biomed. Pharmacother. 108, 1825–1834. https://doi.org/10.1016/j.biopha.2018.09.143.
Wang, N., Xu, T.Y., Zhang, X., Li, J.Y., Wang, Y.X., Guo, X.C., Li, S.M., Wang, W.F., Li, D.S., 2018b. Improving hyperglycemic effect of FGF-21 is associated with alleviating inflammatory state in diabetes. Int. Immunopharmacol. 56, 301–309. https://doi.org/10.1016/j.intimp.2018.01.048.
Wang, Q., Yuan, J., Yu, Z., Lin, L., Jiang, Y., Cao, Z., Zhuang, P., Whalen, M.J., Song, B., Wang, X.J., Li, X., Lo, E.H., Xu, Y., Wang, X., 2018c. FGF21 attenuates high-fat diet-induced cognitive impairment via metabolic regulation and anti-inflammation of obese mice. Mol. Neurobiol. 55, 4702–4717. https://doi.org/10.1007/s12035-017-0663-7.
Woo, Y.C., Xu, A., Wang, Y., Lam, K.S.L., 2013. Fibroblast growth factor 21 as an emerging metabolic regulator: clinical perspectives. Clin. Endocrinol. 78, 489–496. https://doi.org/10.1111/cen.12095.
Wu, X., Qi, Y., Chang, J., Lu, W., Zhang, J., Wang, S., Cheng, S., Zhang, M., Fan, Q., Lv, Y., Zhu, H., Xin, M., Lv, Y., Liu, J., 2015. Possible role of fibroblast growth factor 21 on atherosclerosis via amelioration of endoplasmic reticulum stress-mediated apoptosis in apoE(−/−) mice. Heart Vessel. 30, 657–668. https://doi.org/10.1007/s00380-014-0557-9.
Xie, T., Leung, P.S., 2017. Fibroblast growth factor 21: a regulator of metabolic disease and health span. Am. J. Physiol. Endocrinol. Metab. 313, E292–E302. https://doi.org/10.1152/ajpendo.00101.2017.

Xiong, T., Tang, J., Zhao, J., Chen, H., Zhao, F., Li, J., Qu, Y., Ferriero, D., Mu, D., 2012. Involvement of the Akt/GSK-3β/CRMP-2 pathway in axonal injury after hypoxic–ischemic brain damage in neonatal rat. Neuroscience 216, 123–132. https://doi.org/10.1016/j.neuroscience.2012.04.052.

Yang, X., Hui, Q., Yu, B., Huang, Z., Zhou, P., Wang, P., Wang, Z., Pang, S., Li, J., Wang, H., Lin, L., Li, X., Wang, X., 2018. Design and evaluation of lyophilized fibroblast growth factor 21 and its protection against ischemia cerebral injury. Bioconjug. Chem. 29, 287–295. https://doi.org/10.1021/acs.bioconjchem.7b00588.

Yıldız, E.P., Ekici, B., Tatlı, B., 2016. Neonatal hypoxic ischemic encephalopathy: an update on disease pathogenesis and treatment. Expert. Rev. Neurother. 17, 449–459. https://doi.org/10.1080/14737175.2017.1259567.

Yu, Y., Bai, F., Wang, W., Liu, Y., Yuan, Q., Qu, S., Zhang, T., Tian, G., Li, S., Li, D., Ren, G., 2015. Fibroblast growth factor 21 protects mouse brain against D-galactose induced aging via suppression of oxidative stress response and advanced glycation end products formation. Pharmacol. Biochem. Behav. 133, 122–131. https://doi.org/10.1016/j.pbb.2015.03.020.

Yuan, Y., Zhao, Y., Jia, H., Liu, M., Hu, S., Li, Y., Li, X., 2018. Cortical hemodynamic responses under focused ultrasound stimulation using real-time laser speckle contrast imaging. Front. Neurosci. 12, 269. https://doi.org/10.3389/fnins.2018.00269.

Zalewska, T., Jaworska, J., Ziemka-Nalecz, M., 2015. Current and experimental pharmacological approaches in neonatal hypoxic- ischemic encephalopathy. Curr. Pharm. Des. 21, 1433–1439. https://doi.org/10.2174/1381612820999141029162457.

Zhang, W., Liu, J., Hu, X., Li, P., Leak, R., Gao, Y., Chen, J., 2015. N-3 polyunsaturated fatty acids reduce neonatal hypoxic/ischemic brain injury by promoting phosphatidylserine formation and Akt signaling. Stroke 46, 2943–2950. https://doi.org/10.1161/STROKEAHA.115.010815.

Zhao, X., Wang, H., Sun, G., Zhang, J., Edwards, N., Aronowski, J., 2015. Neuronal Interleukin-4 as a modulator of microglial pathways and ischemic brain damage. J. Neurosci. 35, 11281–11291. https://doi.org/10.1523/JNEUROSCI.1685-15.2015.

Zhou, Z.Q., Li, Y.L., Ao, Z.B., Wen, Z.L., Chen, Q.W., Huang, Z.G., Xiao, B., Yan, X.H., 2017. Baicalin protects neonatal rat brains against hypoxic-ischemic injury by up-regulating glutamate transporter 1 via the phosphoinositide 3-kinase/protein kinase B signaling pathway. Neural Regen. Res. 12, 1625–1631. https://doi.org/10.4103/1673-5374.217335.

Zhu, C., Wang, X., Xu, F., Bahr, B., Shibata, M., Uchiyama, Y., Hagberg, H., Blomgren, K., 2005. The influence of age on apoptotic and other mechanisms of cell death after cerebral hypoxia-ischemia. Cell Death Differ. 12, 162–176. https://doi.org/10.1038/sj.cdd.4401545.